A single-cell transcriptomic atlas reveals resident dendritic-like cells in the zebrafish brain parenchyma

Mireia Rovira[1, 2¶], Giuliano Ferrero[1, 2¶], Magali Miserocchi[1, 2], Alice Montanari[1, 2], Valérie Wittamer[1, 2*]

[1] Institut de Recherche Interdisciplinaire en Biologie Humaine et Moléculaire (IRIBHM), [2] ULB Institute of Neuroscience (UNI), Université Libre de Bruxelles (ULB), Brussels, Belgium

¶ These authors contributed equally to this work

* Author for correspondence: Valerie Wittamer (valerie.wittamer@ulb.be)

KEY WORDS: microglia, macrophages, dendritic cells, zebrafish, *batf3*, *csf1r*, *irf8*

ABSTRACT

Recent studies have highlighted the heterogeneity of the immune cell compartment within the steady-state murine and human CNS. However it is not known whether this diversity is conserved among non mammalian vertebrates, especially in the zebrafish, a model system with increasing translational value. Here, we reveal the complexity of the immune landscape of the adult zebrafish brain. Using single-cell transcriptomics, we characterized these different immune cell subpopulations, including cell types that have not been -or have been poorly- characterized in zebrafish so far. By histology, we found that, despite microglia being the main immune cell type in the parenchyma, the zebrafish brain is also populated by a distinct myeloid population that shares a gene signature with mammalian dendritic cells (DC). Notably, zebrafish DC-like cells rely on *batf3*, a gene essential for the development of conventional DC1 in the mouse. Using specific fluorescent reporter lines that allowed us to reliably discriminate DC-like cells from microglia, we quantified brain myeloid cell defects in commonly used *irf8*$^{-/-}$, *csf1ra*$^{-/-}$ and *csf1rb*$^{-/-}$ mutant fish, revealing previously unappreciated distinct microglia and DC-like phenotypes. Overall, our results suggest a conserved heterogeneity of brain immune cells across vertebrate evolution and also highlights zebrafish-specific brain immunity characteristics.

INTRODUCTION

Over the last years, several landmark studies leveraging high-dimensional techniques have contributed to uncovering the cellular complexity of the human and murine central nervous system (CNS) immune landscapes (Mrdjen et al. 2018; Hammond et al. 2018; Masuda et al. 2019; Van Hove et al. 2019; Jordao et al. 2019; Bottcher et al. 2019). From these works, it was found that, besides parenchymal microglia, the steady-state CNS also harbors diverse leukocytes localized at the CNS-periphery interfaces, including different subtypes of mononuclear phagocytes (MNPs) such as border-associated macrophages (BAMs), monocytes and dendritic cells (DCs)-, along with lymphocytes (T cells, B cells, NK cells or innate lymphoid cells ILCs) and granulocytes (neutrophils). Several of these immune cell populations have since been shown to play important roles in regulating CNS development and homeostasis (Drieu et al. 2022; Pasciuto et al. 2020; Tanabe and Yamashita 2018), or identified as key players in disease models and aging (Alves de Lima et al. 2020; Minhas et al. 2021). Collectively, these studies have highlighted how understanding vertebrate brain leukocyte heterogeneity is key to describe CNS interactions with the microenvironment and other cells such as glial cells, neurons or endothelial cells. In contrast, the CNS immune cell repertoire of other vertebrate models is poorly defined.

This is the case for the zebrafish, an increasingly recognized model for translational research on human neurological diseases, owing to its strong genetics and conserved physiology with mammals (Turrini et al. 2023; Liu 2023; D'Amora et al. 2023). Over the years, the zebrafish has also gained considerable importance in regenerative research due to its remarkable capacities for organ regeneration, including the CNS. While this model has contributed to elucidate important cellular and molecular mechanisms underlying adult brain regeneration (Kizil et al. 2012; Zambusi et al. 2022; Saraswathy et al. 2022), much of the work has largely focused on the neurogenesis side of the equation. However, as it is becoming increasingly clear that inflammation plays key roles in the regeneration process (Kyritsis et al. 2012), attention has recently shifted to non-neuronal brain cell types, especially immune cells. While microglia in the zebrafish adult brain have been identified and characterized in bulk RNAseq studies (Oosterhof et al. 2018; Ferrero et al. 2018; Ferrero et al. 2021; Wu et al. 2020), the phenotypic heterogeneity within the microglial compartment remains unknown. In addition, a complete description of all immune cell populations present in the adult zebrafish brain at steady-state is currently lacking. This is a precondition for studying the complex cellular orchestration that takes place in the healthy and diseased CNS. In an effort to understand the cellular basis of the immune compartment of the zebrafish brain, we have established reliable protocols for dissociation and prospective isolation of brain leukocytes, using fluorescent transgenic lines. By combining this approach with single-cell RNA sequencing, we have generated a gene expression atlas composed of the distinct immune cells present in the homeostatic brain. This dataset revealed the presence of subpopulations of mononuclear phagocytes and other leukocytes, including cell types that have not been -or have been poorly- characterized so far. Here, we present the characterization of a new mononuclear phagocyte population that represents an important fraction among all brain leukocytes and coexist with microglia in the brain parenchyma. This population of cells is *batf3*-dependent and expresses known DC canonical genes. In light of these observations, we have also revisited the phenotype of myeloid-deficient mutant lines, such as *csf1ra*$^{-/-}$, *csf1rb*$^{-/-}$ and *irf8*$^{-/-}$ fish, that have been instrumental to the field. Overall, we provide an overview of the immune landscape in the adult zebrafish brain which, akin to findings in mammals, boasts distinct myeloid and lymphoid cell types.

RESULTS

Mononuclear phagocytes represent the main immune cell population in the adult zebrafish brain

As a first step, we sought to assess the leukocytes present in the zebrafish adult brain according to their cellular morphology. We previously showed the *cd45:DsRe*d transgene labels all leukocytes, with the exception of B lymphocytes (Wittamer et al. 2011; Ferrero et al. 2020). Therefore, we performed May-Grünwald Giemsa (MGG) staining on a pure population of *cd45:DsRed*$^+$ cells isolated from the brain of adult *Tg(cd45:DsRed)* transgenic animals by flow cytometry (**Figure 1A**). Cells with the classical morphological features of mononuclear phagocytes were identified as macrophages/microglia based on their large and vacuolated cytoplasms (Wittamer et al. 2011) (**Figure 1B**). Monocytes, recognized by their kidney-shaped nuclei, were also present, as well as cells with a typical dendritic cell morphology, namely elongated shapes, large dendrites and oval or kidney-shaped nuclei (Lugo-Villarino et al. 2010) (**Figure 1B**). We also found large numbers of lymphocytes, clearly distinguished from myeloid cells by their smaller size and narrow and basophilic cytoplasm stained in blue. The remaining cells were neutrophils, characterized by their clear cytoplasm and highly segmented nuclei.

Next, we took advantage of fluorescent zebrafish transgenic lines, allowing to detect and quantify the different leukocyte subsets using flow cytometry. To achieve this, *Tg(cd45:DsRed)* animals were crossed to established GFP reporters that label mononuclear phagocytes (*Tg(mpeg1:GFP)*), neutrophils (*Tg(mpx:GFP)*, NK and T lymphocytes (*Tg(lck:GFP)*) or IgM-expressing B cells (*Tg(ighm:GFP)*) (**Figure 1A**). As expected, flow cytometry analyses of these double transgenic fish demonstrated that *mpeg1*:GFP$^+$ mononuclear phagocytes were the most abundant leukocytes in the adult brain, accounting for 75.7% ± 2.9 of the total *cd45:DsRed*$^+$ population (n=4) (**Figure 1C,D**). In contrast, *mpx:GFP*$^+$ neutrophils were scarce, representing only 0.2% ± 0.04 of brain leukocytes (n=4) (**Figure 1-supplement 1A**). Regarding lymphocytes, *lck:GFP*$^+$ NK/ T cells were more abundant than *ighm:GFP*$^+$ B cells, accounting for 7.2% ± 0.9 (n=4) and 0.2% ± 0.01 (n=4), respectively (**Figure 1-supplement 1B,C**).

Although *mpeg1*-driven fluorescent transgenes are commonly used to label mononuclear phagocytes, we and others have previously shown that *ighm*-expressing B cells are also marked by these reporters, as they endogenously express *mpeg1.1* (Ferrero et al. 2020; Moyse and Richardson 2020). However, based on the low numbers of brain *ighm:GFP*$^+$ cells identified in our flow cytometry analyses, we concluded their contribution to the *mpeg1*$^+$ population was minimal and that brain *mpeg1*$^+$ cells mostly comprise mononuclear phagocytes. We thus wondered what was the specific proportion of microglial cells within the *mpeg1*$^+$ population. To address this question, we crossed *Tg(cd45:DsRed)* fish to animals carrying the *Tg(p2ry12:p2ry12-GFP)* transgene (Sieger et al. 2012). P2ry12 is an evolutionary conserved canonical microglia marker, including in zebrafish (Mazzolini et al. 2019; Rovira et al. 2022; Ferrero et al. 2018), so its expression can serve to discriminate microglia from other brain macrophages, as shown previously in mammals (Butovsky et al. 2014). Interestingly, analyses of brain cell suspensions from double transgenics showed *p2ry12:GFP*$^+$ microglia accounted for half of *cd45:DsRed*$^+$ cells (50.9 % ± 2.9; n=4) (**Figure 1D,E**). Considering that *mpeg1:GFP*$^+$ cells comprised ~75% of all leukocytes, these results indicated that approximately 25% of brain mononuclear phagocytes do not express the microglial *p2ry12:GFP*$^+$ transgene. Based on our cytological observations, this population likely contains a mixture of monocytes and dendritic cells. Collectively, these analyses suggest an important diversity among leukocytes present in the steady-state brain of the adult zebrafish.

118 **Single-cell transcriptomics identifies multiple leukocyte populations in the adult brain**

119 To fully characterize the heterogeneity within the zebrafish brain immune landscape, next we turned to
120 single-cell trancriptome profiling. Viable *cd45:DsRed*$^{+}$ cells were FACS-sorted from the steady-state brain
121 of adult *Tg(cd45:DsRed)* animals, then subjected to scRNA-sequencing using the 10X platform (**Figure 2A,**
122 **Appendix 1-Figure 2**). After an unsupervised uniform manifold approximation and projection (UMAP) and
123 single-cell clustering, we obtained a total of 20 cell clusters (**Figure 2B**). A preliminary observation of our
124 dataset, revealed the expression of *cd45* (also known as *ptprc*) in all clusters of the dataset, thus
125 confirming their hematopoietic identity (**Figure 2C**). In addition, expression of canonical genes for
126 mononuclear phagocytes (*mpeg1.1*), neutrophils (*mpx*) or T/ NK cells (*lck*, *lymphocyte-specific protein*
127 *tyrosine kinase*) were found in several clusters (**Figure 2C**). Together, these initial observations indicated
128 that we were able to capture a repertoire of different brain leukocytes represented in individual cluster
129 identities. This is in line with the cell type diversity determined from our cytological and flow cytometry
130 analyses.

131 Cluster annotation was achieved based on expression of defined blood lineage-specific genes previously
132 established in zebrafish (Tang et al. 2017; Hernández 2018; Moore et al. 2016), and from published
133 transcriptomes from human and mouse brain leukocytes (Mrdjen et al. 2018; Jordao et al. 2019;
134 Hammond et al. 2018; Masuda et al. 2019; Van Hove et al. 2019). Using these approaches, we were able
135 to annotate 15 clusters. The remaining cells are included in the online material but were not used for
136 further analysis in this study. We identified 7 major leukocyte populations that comprised microglia (MG),
137 macrophages (MF), dendritic-like cells (DC-like), T cells, natural killer cells (NK), innate lymphoid-like cells
138 (ILCs) and neutrophils (Neutro) (**Figure 2B, Table 1**). Expression of the markers for each cluster is
139 visualized plotting the top 50 marker genes (**Figure 2D and Table 2**). Of note, one cluster was annotated
140 as proliferative (Prolif) because of the expression of proliferative markers, suggesting the presence of
141 dividing brain leukocytes, however, marker genes were not indicative of a specific cell type (**Figure 2 B,D**
142 **and Table 1**). A detailed analysis of the different clusters from the lymphoid and myeloid compartments
143 is presented in the following sections, with an emphasis on microglia and DC-like clusters.

144

145 **The adult zebrafish brain contains innate and adaptive lymphoid cells**

146 Expression of *lck*, a conserved marker for T lymphocytes and NK cells (Moore et al. 2016), identified three
147 clusters of lymphoid cells (**Figure 2C, Table 1**). Two of them expressed T cell-specific marker genes such
148 as *zap70* (tcr-associated protein kinase), TCR co-receptors including *cd4-1*, *cd8a*, *cd8b* and *cd28*, and *il7r*,
149 a cytokine receptor that functions in T cell homeostasis (**Figure 3A,D**), all of them showing conservation
150 between mammals and zebrafish. This suggests that these two *zap70*-expressing clusters contain a mix of
151 CD4^{+} and CD8^{+} T cells, and were thus annotated as Tcells1 and Tcells2. Interestingly, a proportion of cells
152 within these clusters expressed *runx3,* which in mammals has been reported as a regulator of tissue
153 resident memory CD8 T cells in different tissues, including the brain (Milner et al. 2017). The second
154 cluster highly expressed genes previously described as markers for NK cells in the zebrafish whole kidney
155 marrow (WKM) (Tang et al. 2017; Carmona et al. 2017), such as chemokines *ccl36.1* and *ccl38.6*,
156 granzymes *gzm3.2* and *gzm3.3*, *il2rb* and *ifng1* (**Figure 3B,D**). However, expression of novel immune-type
157 receptor (*nitr*) or NK-lysin genes was not detected in brain NK cells, in contrast to WKM NK cells (Carmona
158 et al. 2017; Moore et al. 2016; Yoder et al. 2010). Annotation of these lymphoid clusters was mostly based

159 on a zebrafish WKM reference data set (Tang et al. 2017) and therefore, differences may exist between
160 tissues.

161 Notably, we identified an additional cluster that did not express any of the previously mentioned T cell
162 markers but displayed *il4* and *il13* expression in a large proportion of cells (**Figure 3C,D**). In mammals,
163 these two cytokines identify $CD4^+$ T helper type 2 cells as well as innate-lymphoid cells type 2 (ILC2s), the
164 innate counterparts of adaptive T helper cells (Vivier et al. 2018). Interestingly, this cluster was also
165 positive for *gata3*, a transcription factor that regulates the development and funcions of ILC2s (Wong et
166 al. 2012). The expression profile identified in this cluster may thus represent the molecular signature of
167 zebrafish ILC2-like cells (Vivier et al. 2016). To test this hypothesis, we performed qPCR analyses on
168 *cd45:DsRed*$^+$ brain cells isolated from *rag2*-deficient fish. We hypothesized that, like their murine
169 counterparts (Spits and Cupedo 2012), *rag2* mutant zebrafish, which lack T and B cells (Tang et al. 2014),
170 would still produce ILC-like cells. Supporting this postulate, while the expression levels of *lck* and *zap70*
171 was significantly reduced in brain leukocytes from the *rag2* mutants in comparison with that from their
172 *wild-type* siblings (**Figure 3E**), *gata3*, *il4* and *il13* showed similar expression levels between cells from both
173 genotypes (**Figure 3E**). It thus appears that the expression of putative ILC2 cell-associated genes in brain
174 leukocytes is not changed in the absence of T cells. Altogether, these findings support our annotation of
175 this cluster as ILC-like cells.

176

177 **The adult brain contains other mpeg1-expressing cells beside microglia**

178 As shown in **Figure 2C**, expression of *mpeg1.1*, a canonical marker for mononuclear phagocytes, was
179 identified in nine clusters of our dataset. Four clusters were annotated as microglia (MG), one as
180 macrophages (MF) and four as dendritic-like cells (DC-like) (**Figure 2B and Table 1**).

181 MG clusters (MG1, MG2, MG3, MG4) differentially expressed zebrafish microglial genes such as the
182 lipoproteins *apoc1* and *apoeb* (Herbomel, Thisse, and Thisse 2001; Peri and Nusslein-Volhard 2008;
183 Ferrero et al. 2018; Mazzolini et al. 2019), *ms4a17a.10* (Oosterhof et al. 2018) - a member of the
184 membrane-spanning 4A gene family-, galectin 3 binding protein *lgals3bpb* (Rovira et al. 2022; Kuil et al.
185 2019), and hepatitis A virus cellular receptors *havcr1* and *havcr2* (Kuil et al. 2019; Oosterhof et al. 2018)
186 (**Figure 4A,D**). Moreover, *csf1ra* and *csf1rb,* the zebrafish paralogs of CSF1R and well conserved regulators
187 of microglia development and homeostasis (Oosterhof et al. 2018; Ferrero et al. 2021; Hason et al. 2022),
188 were also identified as marker genes, although their level of expression differed between microglia
189 clusters (**Figure 4D, Table 1**). Importantly, expression of canonical microglial genes were also found in the
190 MG clusters such as *p2ry12*, *hexb*, *mertka* and members of the *c1q* genes, among others, supporting a
191 conserved microglial phenotype (Butovsky et al. 2014; Jurga, Paleczna, and Kuter 2020; Butovsky and
192 Weiner 2018; Gerrits et al. 2020) (**Figure 4-supplement 1**).

193 We also found a cluster of *mpeg1.1*-expressing cells that we annotated as *non-microglia macrophages*
194 (MF). Similar to the microglia clusters (MG), this cluster differentially expressed macrophage-related
195 genes such as *marco*, *mfap4, csf1ra* and components of the complement system (e.g. *c1qb*) (**Figure 4B,D,**
196 **Table 1**). However, this cluster differed from the four microglia clusters because microglia markers were
197 not found. This cluster also showed high expression of calcium binding proteins such as *s100a10b*, *anxa5b*
198 and *icn,* as well as the coagulation factor XIII *f13a1b*, among others (**Figure 4B,D and Table 1**). In contrast
199 to mammals, the distinction between microglia and other macrophages in the adult zebrafish brain (i.e.

200 border-associated macrophages) is still unclear (Silva et al. 2021) and to date, no known marker or
201 fluorescent reporter line is available to distinguish these two related cell types. Another possibility is that
202 these *mpeg1.1*-expressing cells are blood-derived macrophages. In order to better characterize these two
203 *mpeg1.1*-expressing clusters we performed a differential expression analysis between MF and MG (all
204 four clusters together). As shown in **Figure 4E**, microglial genes such as *apoeb*, *apoc1*, *lgals3bpb*, *ccl34b.1*,
205 *havcr1* and *csf1rb* were significantly down-regulated, whereas macrophage-related genes such as
206 *s100a10b*, *sftpbb*, *icn*, *fthl27*, *anxa5b*, *f13a1b* and *spi1b* were significantly up-regulated (**Table 3**).
207 Therefore, these genes may thus serve as novel markers to discriminate these two related types of
208 macrophages.

209 Finally, our analysis identified a third group of *mpeg1.1*-expressing cells represented in four clusters (DC1,
210 DC2, DC3, DC4) and annotated as DC-like (**Figure 2B**). Highly expressed genes in these clusters included
211 *siglec15l* (sialic acid binding Ig-like lectin 15, like) and *ccl19a.1* (C-C motif ligand 19a), a putative ligand of
212 the zebrafish T cell receptor *ccr7* (Wu et al. 2012) (**Figure 4C,D and Table 1**). Intriguingly, these four
213 clusters expressed *id2a*, *xcr1a.1*, *batf3* (*basic leucine zipper ATF-like 3 transcription factor*), and *flt3*
214 (**Figure 4C,D and Table 1**), which are the orthologs of the mammalian Id2a, Xcr1, Batf3 and Flt3 genes,
215 required for development and/or functions of conventional dendritic cells (cDC1) (Cabeza-Cabrerizo et al.
216 2021). These clusters also expressed *chl1a* (adhesion molecule L1), reported to promote DC migration
217 through endothelial cells (Maddaluno et al. 2009) and *hepacam2* (**Figure 4D, Table 1**), frequently found
218 in mammalian DC expression datasets. However, all four clusters had negligible expression of any of the
219 microglia or macrophage markers previously mentioned (**Figure 4D, Table 1**). Based on their transcription
220 profile and possible shared characteristics with mammalian DCs, these clusters were annoted as DC-like
221 cells (DC1, DC2, DC3, DC4).

222 We next conducted a differential expression analysis of DC-like cells (DC1, DC2, DC3, DC4) versus MG
223 (MG1, MG2, MG3, MG4), as two separate clusters. As shown in **Figure 4F**, significantly different genes
224 include genes previously found as DC-like (up-regulated) or microglial (down-regulated) markers, thus
225 confirming their distinct transcriptomic profiles. In addition DC-like cells could also be identified based on
226 differential expression of *irf8*, *ptprc* and *mpeg1.1*, all significantly up-regulated in this population in
227 comparison to MG (**Figure 4F, Table 3**). This is similar to mammalian cDC1, which are IRF8^{high},
228 PTPRC(CD45)^{high} and MPEG1^{high} (Cabeza-Cabrerizo et al. 2021), and thus strenghtens the idea that DC-like
229 cells phenotypically resemble mammalian cDC1. In order to explore the biological function of MG and DC-
230 like cells, we performed pathway enrichment analysis (using GO Biological Processes and Reactome) for
231 each MG and DC-like markers (**Table 4 and see Materials and Methods**). This analysis enriched for terms
232 in MG such as *endosomal lumen acidification* (e.g. H+ ATPase family genes), *synapse pruning* (e.g.
233 C1QC/*c1qc*), *response to lipoprotein particle* (e.g. ABCA1/*abca1b*, APOE/*apoeb*), *interleukin-10 signalling*
234 (e.g. IL10RA/*il10ra*), *macrophage activation* (e.g. CTSC/*ctsc*, HAVCR2/havcr2), *MHC class II antigen*
235 *presentation* (e.g. CD74/*cd74a*, HLA-DOB/mhc2b), *complement cascade* (e.g. C1QA/*c1qa*, CFP/cfp),
236 *mononuclear cell migration* (e.g. CSF1R/*csf1rb*, CMKLR1/*cmklr1*) or *phagocytosis* (e.g. MERTK/*merkta*,
237 MARCO/*marco*) (**Figure 4 supplement 2A, Table 4 and see Materials and Methods**). Enriched terms in
238 DC-like included *FLT3 signaling* (e.g. FLT3/flt3), *myeloid cell differentiation* (e.g. BATF3/batf3, ID2/*id2a*),
239 *Rac2 GTPase cycle* (e.g. RAC2/*rac2*, CDC42/*cdc42l*), *Fc receptor signaling pathway* (e.g. FCER1G/*fcer1g*),
240 *cell chemotaxis* (e.g. CCL19/*ccl19a.1*, XCR1/*xcr1a.1*), innate signaling pathways such as *toll-like receptor*
241 *cascades* (e.g. TLR6/*tlr1*, IRAK3/*irak3*) as well as terms involved in adaptive immunity such as *alpha-beta*
242 *T cell activation* (e.g. CBLB/*cblb*, SOCS1/*socs1*) or *lymphocyte activation involved in immune response* (e.g.

243 *IL12B/il12ba*) (**Figure 4-supplement 2B**). Moreover, we used the Enrichr tool to predict the annotation of
244 the MG and DC-like clusters using the PanglaoDB database that contains multiple single-cell RNA
245 sequencing experiments from mouse and human (Franzen, Gan, and Bjorkegren 2019). The three top
246 significant cell types for MG marker genes were "microglia", "monocytes" and "macrophages" while for
247 DC-like were "Dendritic Cells", "Plasmacytoid DCs" and "Langerhans Cells" (**Figure 4-supplement 2C,D**).

248

249 **DC-like cells as a parenchymal population along with microglia**

250 Having demonstrated the diversity of the immune landscape of the adult zebrafish brain, we next sought
251 to investigate the tissue localization of the different leukocyte populations identified in our data set, using
252 the same transgenic lines as in **Figure 1**. To differentiate microglia from the two phenotypically distinct
253 populations of brain mononuclear phagocytes (MF and DC-like), we first examined adult brain sections of
254 *Tg(mpeg1:GFP)* and *Tg(p2ry12::p2ry12-GFP)* single transgenic fish immunolabeled for GFP and the pan-
255 leukocytic marker L-plastin (Lcp1). We found the majority of L-plastin$^+$ cells within the brain parenchyma
256 co-expressed the *mpeg1:GFP* transgene (**Figure 5A-C**). Upon examination of *Tg(p2ry12:p2ry12-GFP)* fish,
257 however, we observed that not all parenchymal L-plastin$^+$ cells were GFP (**Figure 5D-F**). Analysis of
258 *Tg(p2ry12:p2ry12-GFP; mpeg1:mCherry)* double transgenics confirmed these observations, a.k.a that a
259 fraction of *mpeg1:mCherry*$^+$ cells was negative for the microglial *p2ry12:p2ry12-GFP* transgene (**Figure 5G-**
260 **J**). Interestingly, in contrast to GFP$^+$; mCherry$^+$ microglia which are abundant across brain regions, GFP$^-$
261 mCherry$^+$ cells particularly localized in the ventral part of the posterior brain parenchyma (midbrain and
262 hindbrain) (**Figure 5G-J**). Notably, these cells presented with a highly branched morphology when
263 compared to GFP$^+$; mCherry$^+$ microglia.

264 Based on these findings, we next investigated brain samples from *Tg(mhc2dab:GFP; cd45:DsRed)* fish,
265 where co-expression of both fluorescent reporters specifically labels mononuclear phagocytes (Wittamer
266 et al. 2011; Ferrero et al. 2018). In our previous work, we had already observed that, in the brain of these
267 animals, two phenotypically distinct cell populations could be isolated by flow cytometry based on
268 differential *cd45:DsRed* expression levels. While the *cd45*^{low}; *mhc2*$^+$ fraction was clearly identified as
269 microglia due to their specific expression of *apoeb* and *p2ry12*, the exact identity of the *cd45*^{high}; *mhc2*$^+$
270 cells remained unclear. However, we initially found these cells lack expression of *csf1ra* transcripts
271 (Ferrero et al. 2018) which, in light of our single cell transcriptomic data, excluded them as macrophages
272 and point to a DC-like cell identity. So, to evaluate the tissue localization of *cd45*^{high}*; mhc2*$^+$ cells, we
273 performed direct imaging of transgene fluorescence on vibratome brain sections from *Tg(mhc2dab:GFP;*
274 *cd45:DsRed)* fish (**Figure 5K**). Most GFP$^+$ cells were DsRed negative, suggesting the low expression of the
275 *cd45* transgene in microglia likely precluded direct imaging of DsRed in these cells. However, in the ventral
276 part of the posterior brain (midbrain and hindbrain), we observed a clear population of GFP$^+$; DsRed$^+$ cells,
277 with a highly ramified morphology (**Figure 5L-N**). The reliable detection of endogeneous DsRed signal in
278 these cells likely identified them as DsRed^{high}. Altogether, these observations strongly pointed to *mpeg1*$^+$*;*
279 *p2ry12*$^-$ and *cd45*^{high}*; mhc2*$^+$ cells as being the same parenchymal non microglial population.

280 Finally, we also examined the localization of neutrophils and lymphoid cells, labeled using the
281 *Tg(mpx:GFP)*, *Tg(lck:GFP)* and *Tg(ighm:GFP)* lines, respectively (**Figure 5-supplement 1**). In accordance
282 with *mpeg1*$^+$*; Lcp1*$^+$ cells being the main leukocyte population present in the adult zebrafish brain
283 parenchyma and with our previous flow cytometry analysis, *mpx*$^+$, *lck*$^+$ and *ighm*$^+$ cells were rarely found

284 and, if present, they were located at the border of the sections or lining the ventricles (**Figure 5-**
285 **supplement 1**).

286 Collectively, our findings demonstrated that, in addition to microglia, the steady-state brain parenchyma
287 of the adult zebrafish brain contains phenotypically distinct populations of mononuclear phagocytes with
288 a restricted spatial localization within the tissue. Importantly, these two populations are easily
289 distinguished using a combination of available transgenic lines.

290

291 **Transcriptomic analysis of microglia and DC-like cells sorted using different reporter lines**

292 To determine whether brain *mpeg1:mCherry*$^{+}$*; p2ry12:GFP*$^{-}$ and *cd45:DsRed*^{high}*; mhc2:GFP*$^{+}$ cells do indeed
293 represent a unique population of DC-like cells, we next performed bulk transcriptomic analyses to
294 compare their expression profile. As a source for these studies, we used both *Tg(p2ry12::p2ry12-GFP;*
295 *cd45:DsRed)* and *Tg(mhc2dab:GFP; cd45:DsRed)* adult fish, allowing to FACS-sort microglia identified in
296 these animals as GFP^{+}; DsRed^{+} or GFP^{+}; DsRed^{low} cells, respectively (Ferrero et al. 2018). Brain putative DC-
297 like cells were obtained using the *Tg(mhc2dab:GFP; cd45:DsRed)* reporter, and isolated as GFP^{+}; DsRed^{high}
298 (**Figure 6A-C**).

299 Differential expression analysis between *mhc2dab:GFP*$^{+}$*; cd45:DsRed*^{high} – or putative DC-like cells- and
300 *p2ry12:GFP*$^{+}$*; cd45:DsRed*$^{+}$ - or microglia- showed up-regulation of DC-like genes previously found in our
301 single-cell transcriptomic analysis (**Figure 6D, Table 5**). Similar results were obtained when comparing DC-
302 like cells with microglia FACS-sorted as *mhcdab*$^{+}$; *cd45*$^{+}$ cells (**Figure 6E, Table 5**). These analyses confirm
303 that our annotated DC-like cluster and *cd45:DsRed*^{high}*; mhc2dab:GFP*$^{+}$ cells share a similar transcriptome
304 distinct from microglia.

305 Interestingly, a recent study reported the presence of two heterogenous populations of *mpeg1*-expressing
306 cells in the adult zebrafish brain. These cells, which were annotated as *phagocytic* and *regulatory*
307 microglia, and could be discriminated based on differential expression of the *ccl34b.1:GFP* reporter (Wu
308 et al. 2020). Interestingly, these two populations displayed a similar morphology, neuroanatomical
309 location and differential gene expression pattern than the annotated DC-like and microglia populations
310 identified in our dataset. We thus re-analyzed the data from Wu et al.. Differential expression between
311 *regulatory* (*ccl34b.1*$^{-}$; *mpeg1*$^{+}$) and *phagocytic* (*ccl34b.1*$^{+}$; *mpeg1*$^{+}$) cells demonstrated up-regulation of
312 genes such as *siglec15l*, *spock3*, *chl1a*, *flt3*, *hepacam2*, *ccl19a.1*, *id2a* and *epdl1*, and down-regulation of
313 genes such as *p2ry12*, *ccl34b.1*, *apoeb*, *apoc1*, *lgals3bpb*, *lgals9l1* and *havcr1*, among others (**Figure 6-**
314 **supplement 1A and Table 5**). Notably, a large proportion of these DE genes overlapped with that
315 previously found when comparing *mhc2dab:GFP*$^{+}$*; cd45:DsRed*^{high} DC-like cells and *p2ry12:GFP*$^{+}$*;*
316 *cd45:DsRed*$^{+}$ microglia (**Figure 6-supplement 1B,C and Table 5**). B cell-related genes such as *ighz* and *pax*
317 were up-regulated (**Figure 6-supplement 1A**), suggesting the presence of B cells in the *ccl34b.1*$^{-}$; *mpeg1*$^{+}$
318 fraction, as expected (Ferrero et al. 2020; Moyse and Richardson 2020). In addition, the expression profile
319 of *ccl34b.1*$^{+}$; *mpeg1*$^{+}$ *phagocytic* microglia strongly correlated with that of *p2ry12:GFP*$^{+}$*; cd45:DsRed*$^{+}$ and
320 *mhc2dab:GFP*$^{+}$; *cd45:DsRed*$^{+}$ microglia (0.76 and 0.71, respectively), whereas *ccl34b.1*$^{-}$; *mpeg1*$^{+}$ *regulatory*
321 microglia correlated with *mhc2dab:GFP*$^{+;}$ *cd45:DsRed*^{high} DC-like cells (0.57) (**Figure 6-supplement 1D,E**
322 **and Table 5**). Collectively, these findings suggest that, at the transcriptomic level, *ccl34b.1*$^{+}$*; mpeg1.1*$^{+}$ cells
323 correspond to microglia in our dataset, and *ccl34b.1*; $^{-}$*mpeg1*$^{+}$ cells resemble the population we annotated
324 as DC-like cells.

325

326 **DC-like cells are located in the brain parenchyma and are *batf3*-dependent**

327 Our results so far suggested the existence of a putative DC-like cell population located in the parenchyma
328 of the healthy zebrafish brain. To strenghten our findings, we next developed a strategy to assess the
329 identity of this population. We reasoned that the development of the zebrafish counterparts of
330 mammalian cDC1 would likely rely on a conserved genetic program. In our single-cell transcriptomic
331 analysis, zebrafish DC-like cells expressed *batf3*, a cDC1-required transcription factor in human and mouse
332 (Cabeza-Cabrerizo et al. 2021). Therefore, using CRISPR/Cas9 technology we generated a zebrafish *batf3*
333 mutant as a model to explore the lineage identity of putative zebrafish DC-like cells. This mutant line
334 carries a 8-bp deletion downstream of the ATG start, leading to a frameshift mutation and the generation
335 of three premature stop codons (**Appendix 2-Figure 7**). The resulting protein lacks the DNA binding and
336 basic-leucine zipper domains and is likely to be non-functional. To evaluate whether brain DC-like cells
337 were present in these animals, we crossed the *batf3* mutant line to *Tg(p2ry12:p2ry12-GFP;*
338 *mpeg1:mCherry)* double transgenic fish, and performed immunostainings of adult brain sections (**Figure**
339 **7A-J**). Because DC-like cells are abundant in the ventral posterior brain, we quantified the dorsal (mostly
340 containing the optic tectum) and ventral areas separately, as well as the whole section. The numbers of
341 GFP^+; $mCherry^+$; $Lcp1^+$ microglia were similar to their *wild-type* siblings, whereas the ventral posterior
342 brain of homozygous *batf3* mutants was largely devoid of GFP^-; $mCherry^+$; $Lcp1^+$ cells, which identify DC-
343 like cells in our model (**Figure 7K-M**). Moreover, we did not observe any changes in the density of other
344 brain leukocytes (**Figure 7-supplement 1A-C**). Flow cytometry analyses of brain cell suspensions
345 confirmed the dramatic loss of GFP^-; $mCherry^+$ cells in the absence of *batf3* (2.98% ± 0.588, n=6 versus
346 0.77 ± 0.097, n=10) (**Figure 7 N,O**). Notably, expression of DC-like markers was barely detectable in the
347 remaining GFP^-; $mCherry^+$ cells (**Figure 7-supplement 1D,E**). However, these cells also displayed lower
348 mCherry signal intensity, suggesting they most likely represent *mpeg1*-expressing MF or B cells (**Figure 7-**
349 **supplement 1F,G**). Regarding GFP^+; $mCherry^+$ microglia, their proportion was unchanged when compared
350 to that of control fish (**Figure 7 N,O**), which is concordant with our initial observations. Finally, we also
351 performed direct imaging of transgene fluorescence on vibratome brain sections of *batf3* mutants
352 carrying the *cd45:DsRed* transgene. In line with our observations, we found that loss-of-function of *batf3*
353 in *Tg(cd45:DsRed)* transgenic fish resulted in the complete absence of $DsRed^{high}$ DC-like cells in the ventral
354 area of the midbrain parenchyma in comparison with control brains (**Figure 7-supplement 1H-K**).
355 Collectively, these results demonstrated that, the population we annotated as DC-like cells is *batf3*-
356 dependent similar to mammalian cDC1. These results reinforced our hypothesis that these cells represent
357 the zebrafish counterparts of mammalian cDC1.

358

359 **Characterization of microglia and dendritic-like cells in mononuclear phagocyte-deficient mutants.**

360 The presence of two distinct mononuclear phagocyte subsets in the brain parenchyma made us wondered
361 about their respective status in commonly used microglia-deficient zebrafish lines, as they were all initially
362 characterized using the pan-mononuclear phagocyte *Tg(mpeg1:GFP)* reporter **(Oosterhof et al. 2018;**
363 **Ferrero et al. 2021; Wu et al. 2020)**. With the ability to discriminate between both populations of
364 microglia and DC-like cells, we thus next sought to examine in more details the phenotype of the *irf8*$^{-/-}$,
365 *csf1ra*$^{-/-}$, *csf1rb*$^{-/-}$ and *csf1ra*$^{-/-}$; *csf1rb*$^{-/-}$ double mutant (*csf1r*^{DM}) alleles. To do so, we crossed each mutant
366 line to *Tg(p2ry12:p2ry12-GFP)* animals and analyzed brain sections costained for GFP and L-plastin (**Figure**

367 **8**). According to our model, in this setup microglia will be labeled as GFP$^+$; Lcp1$^+$, while GFP$^-$; Lcp1$^+$ cells
368 will mostly include DC-like cells, easily identified based on their typical ramified cell shape (**Figure 8A-D**).
369 In addition to DC-like cells, GFP$^-$; Lcp1$^+$ cells may also include lymphocytes and/or neutrophils, which are
370 anyway in much lower numbers than mononuclear phagocytes in the adult brain (**Figure 1D**).

371 IRF8 is a transcription factor essential for the development of mononuclear phagocytes in vertebrates
372 (Yanez and Goodridge 2016), including zebrafish (Ferrero et al. 2020), where absence of *irf8* results in lack
373 of microglia (Shiau et al. 2015; Earley, Graves, and Shiau 2018). In line with these findings, we found that
374 adult *irf8* homozygous displayed a dramatic, albeit not complete, reduction of GFP$^+$ microglial cells (**Figure**
375 **8E-H, U,W**). Interestingly, most remaining microglia localized near or along the ventricle borders, and
376 exhibited characteristics reminescent of an immature phenotype, e.g. a circular shape with few and short
377 cellular processes (**Figure 8-supplement 1**). In this mutant, the density of GFP$^-$; Lcp1$^+$ DC-like cells was
378 reduced in comparison to *wild-type* controls, in the ventral area (~50%) (**Figure 8U,W**).

379 As well-established regulators of zebrafish microglia, *csf1ra* or *csf1rb* deficiency had a strong effect on
380 GFP$^+$; Lcp1$^+$ cells, with densities decreased ~50% in the dorsal and ventral areas. Interestingly, the density
381 of GFP$^-$; Lcp1$^+$ DC-like cells was reduced in the ventral part of *csf1rb* homozygous fish (~50%), while it was
382 doubled in *csf1ra*$^{-/-}$ mutant animals in comparison to *wild-type* siblings (**Figure 8I-P, U,W**). Finally, we also
383 examined fish lacking both *csf1r* paralogs (*Csf1r*^{DM}). These fish displayed a more severe phenotype, being
384 devoid of both populations of microglia and DC-like cells, as indicated by the absence of GFP and Lcp1
385 signal (**Figure 8Q-W**). This is consistent with previous reports that *mpeg1:GFP*$^+$ cells are depleted in the
386 brain of *csf1r*^{DM} fish (Ferrero et al. 2021; Oosterhof et al. 2018).

387 Collectively, these results demonstrate the different mononuclear phagocyte-deficient zebrafish mutant
388 lines have reduced numbers of microglia and exhibit distinct DC-like cell phenotypes. Our data also reveal
389 that DC-like cells develop in an *irf8*-dependant manner, and identify possible opposite functions for the
390 *csf1r* paralogs in the maintenance of this population.

391

392 **DISCUSSION**

393 In the present study, we have characterized the immune microenvironment of the adult zebrafish brain
394 by profiling total cd45$^+$ leukocytes, isolated from transgenic reporter fish by FACS. First we show that, like
395 in mammals, microglia constitute the predominant parenchymal immune cell in the brain of the adult
396 zebrafish. Zebrafish microglia are identified based on several common canonical markers, some of which
397 are previously reported to be conserved in mammals (Mazzolini et al. 2019; Silva et al. 2021; Oosterhof et
398 al. 2018). These include *apoeb*, *apoc1*, *lgals3bpb*, *ccl34b.1* and *p2ry12*. Notably, we used different
399 combinations of fluorescent reporter lines for the prospective isolation of adult microglia and found these
400 genes to be consistently expressed. In addition, our observations also support a phenotypical
401 heterogeneity of adult zebrafish microglia in the steady state by identifying several clusters sharing this
402 microglia core signature, with different expression levels. This is in line with recent advances in our
403 understanding of microglia diversity in human and mouse, and which revealed the presence of
404 molecularly distinct microglia subtypes across developmental stages, specific brain regions or disease
405 conditions (Stratoulias et al. 2019; Masuda et al. 2020).

406 Although the notion of microglia heterogeneity in zebrafish is already proposed (Silva et al. 2021; Wu et
407 al. 2020), a major finding of our study is that, surprisingly, not all parenchymal mononuclear phagocytes

408 qualify as microglial cells. Here we provide evidence that a proportion of myeloid cells in the healthy brain
409 parenchyma is phenotypically distinct from microglia and identify as the zebrafish counterpart of
410 mammalian cDC1. These cells, despite sharing the microglial expression of *mpeg1.1* and genes involved
411 in antigen presentation, display a unique transcriptomic profile characterized by a core gene signature
412 resembling that of mammalian cDC1 (*flt3*$^{+}$*, irf8*^{high}*, batf3*$^{+}$*, id2*$^{+}$*, xcr1*$^{+}$) but lacking canonical microglia
413 markers. The lineage identity of these cells (referred to as DC-like cells), is further supported by their
414 dependency to *batf3*, a key transcription factor for cDC1 development in mammals. In contrast, zebrafish
415 microglia develop normally in absence of *batf3*, which highlights the reliance of both populations on
416 distinct developmental programs. This notion is also reinforced by demonstrating that, unlike microglia,
417 zebrafish brain DC-like cells are *csf1ra*-independant. However, both populations are controlled by *irf8*, a
418 well-established regulator of microglia differentiation and DC development in mammals (Van Hove et al.
419 2019; Cabeza-Cabrerizo et al. 2021).
420

421 Previously, two independent studies have reported the existence of an immune cell population with a
422 similar expression profile to DC-like cells in the juvenile and adult zebrafish brain (Wu et al. 2020; Silva et
423 al. 2021). However, contradictory conclusions were drawn regarding the identity of these cells. In one
424 study using bulk RNAseq, a cell population expressing *id2a*, *ccl19a.1*, *siglec15l*, but not *apoeb* or *lgals3bpb*,
425 was identified and categorized as a phenotypically distinct microglia subtype (Wu et al. 2020). This
426 population could be discriminated from other *mpeg1*-expressing parenchymal cells notably by the lack of
427 Tg(*ccl34b.1:GFP*) transgene expression. Interestingly, while *ccl34b.1*$^{+}$; *mpeg1*$^{+}$ microglia were widely
428 spread across brain regions, *ccl34b.1*$^{-}$ *mpeg1*$^{+}$ cells showed a restricted spatial localization in the white
429 matter. In addition, these cells also displayed a highly ramified morphology as well as independency of
430 *csf1ra* signaling, all reminescing the DC-like cells identified in our study. However, in another report using
431 single-cell RNAseq, a comparable myeloid population expressing high levels of *mpeg1* as well as *ccl19a.1*,
432 *flt3*, *siglec15l*, among other DC-like genes, was labeled as brain macrophages, owing to the absence of
433 microglial-specific markers such as *p2ry12*, *csf1ra*, *hexb* and *slc7a7* (Silva et al. 2021). The present work
434 resolves these apparent contradictions, and provides new insights into the identity of this cell population.
435 We report here that *ccl34b.1*$^{-}$*; mpeg1*$^{+}$ cells display a similar gene signature to the DC-like cells identified
436 in our analyses. This strongly suggests that the *ccl34b.1*$^{-}$*; mpeg1*$^{+}$ and *p2ry12*$^{-}$*; mpeg1*$^{+}$ populations share
437 a similar cellular identity. Likewise, the anatomical location of the brain macrophage cluster identified by
438 Silva and colleagues was not investigated, but based on their dominated expression profile by key DC
439 markers, these cells likely represent the equivalent of the *p2ry12*$^{-}$*; mpeg1*$^{+}$ cell population. Thus, based
440 on the evidence that these three populations constitute a unique cell type, and coupled to the
441 demonstration that *in vivo p2ry12*$^{-}$*; mpeg1*$^{+}$ cells are reliant on *batf3*, collectively these features imply
442 these cells share more similarities with mammalian DCs than with microglia or macrophages. Therefore,
443 with respect to their morphology, transcriptomic profile and *batf3*-dependency, we propose this
444 population as DC-like cells rather than microglia and/or macrophages.

445 One important question raised from these new findings could relate to the abundance of DC-like cells
446 within the healthy zebrafish brain parenchyma, which is strongly different than what is known in
447 mammals. Indeed, while murine DCs are naturally found at the brain border regions such as the meningeal
448 layers and the choroid plexus – structures in contact with the brain microenvironment- (Van Hove et al.
449 2019) their presence within the healthy brain parenchyma is scarce and somewhat controversial. In
450 mammals, infiltration of functional DCs in the brain parenchyma occurs with age (Kaunzner et al. 2012),
451 or following an injury or infection, where they act as important inducers of the immune response through

452 activation of primary T cells and cytokine production (Ludewig et al. 2016). In addition, DC infiltration is a
453 hallmark of several neurological diseases and aging, and is believed to contribute to the establishment of
454 a chronic neuroinflammatory state (Ludewig et al. 2016). In this regard, Wu et al. previously reported that
455 *ccl34b.1*$^{-}$ *mpeg1*$^{+}$ cells - or DC-like cells - exhibit functional differences, including limited mobility and
456 phagocytic properties, and enhanced release of immune regulators following bacterial infection, when
457 compared to *ccl34b.1*$^{+}$ *mpeg1*$^{+}$ microglia. The same study also proposed that zebrafish *ccl34b.1*$^{-}$*; mpeg1*$^{+}$
458 cells might play a regulatory role by recruiting T lymphocytes in the brain parenchyma upon infection (Wu
459 et al. 2020). These biological features suggest that brain DC-like cells might exibit APC functions. However,
460 due to a lack of tools this hypothesis is currently difficult to address. There is evidence that DC
461 functionalities are conserved in teleosts (Lugo-Villarino et al. 2010; Bassity and Clark 2012), but the
462 process of antigen presentation in zebrafish remains poorly understood (Lewis, Del Cid, and Traver 2014).
463 Because zebrafish lack apparent lymph nodes and the secondary lymphoid structures found in mammals,
464 it is not known where stimulation of naive T cells takes place and whether fish have developped unique
465 ways to mount an adaptive immune response. Therefore, although a comprehensive analysis of the
466 anatomical zone enriched in DC-like cells requires further investigation, from an evolutionary perspective,
467 it is tempting to speculate that the specific localization of zebrafish DC-like cells in the ventral brain tissue
468 might provide an environment to facilitate antigen detection and/or presentation in this organ. Future
469 work using the mutants as described in this study in addition to new DC-like-specific reporter lines will
470 help addressing such exciting questions.

471 Furthermore, our work sheds light on the myeloid brain phenotype of mutant lines commonly used by
472 the fish macrophage/microglia community. CSF1R is a master regulator of macrophage development and
473 function in vertebrates which is found in two copies (*csf1ra* and *csf1rb*) in zebrafish due to an extra
474 genome duplication. Others and we have contributed to the uncovering of the relative contribution of
475 each paralog to the ontogeny of zebrafish mononuclear phagocytes (Herbomel, Thisse, and Thisse 2001;
476 Ferrero et al. 2021; Hason et al. 2022; Oosterhof et al. 2018). Here we also provide a new level of precision
477 regarding these processes. As reported, the density of all parenchymal *mpeg1:GFP*$^{+}$ mononuclear
478 phagocytes is reduced in the brain of single *csf1ra*$^{-/-}$ and *csf1rb*$^{-/-}$ adult mutant fish, and these cells
479 completely disappear when both genes are knocked out (Oosterhof et al. 2018; Ferrero et al. 2021). Using
480 *in vivo* lineage tracing, we previously demonstrated that zebrafish microglia are established in two
481 successive steps, with a definitive wave of hematopoietic stem cell (HSC)-derived adult microglia replacing
482 an embryonic/primitive population. In addition, we showed that in *csf1rb*$^{-/-}$ fish remaining *mpeg1:GFP*$^{+}$
483 cells are of primitive origin, whereas in *csf1ra*$^{-/-}$ fish they are of definitive origin (Ferrero et al. 2021).
484 Collectively, these observations have led to a model in which embryonic-derived microglia make up the
485 majority of remaining *mpeg1*-expressing cells in *csf1rb*$^{-/-}$ fish, while residual cells represent adult microglia
486 in the *csf1ra*$^{-/-}$ line, but at a strongly reduced cell number relative to controls. However, adult microglia in
487 these experiments were identified based on the concomitant *mpeg1:GFP* transgene expression and the
488 HSC lineage tracing marker, a strategy that, retrospectively, did not allow to discriminate them from the
489 DC-like cells described in this study. Here, we sought to test these models in light of our current findings,
490 and especially following the observation that individual mutant fish exhibit opposite brain DC-like
491 phenotypes, with DC-like cell numbers being strongly increased or decreased in *csf1ra*$^{-/-}$ and *csf1rb*$^{-/-}$
492 animals, respectively. In mammals, DCs are produced by HSCs in the bone marrow so the reduced
493 numbers of DC-like cells in *csf1rb*$^{-/-}$ fish likely results from the defective HSC-derived definitive
494 myelopoiesis that characterized this mutant (Ferrero et al. 2021; Hason et al. 2022). Accordingly, the
495 *csf1rb*$^{-/-}$ line is devoid of both populations of adult microglia and DC-like cells and, as initially proposed,

496 the most residual cells within the brain parenchyma represent remnants of embryonic microglia (Ferrero
497 et al. 2021). Conversely, the increased density of DC-like cells in *csf1ra*$^{-/-}$ adult fish indicates that this
498 paralogue is dispensable for the ontogeny of DC-like cells, but points to a possible role in controlling the
499 DC-like cell growth and/or survival. This is in contrast with microglia, which we now found to be
500 unambiguously depleted following a *csf1ra* loss-of-function. Therefore, these findings warrant an
501 adjustment of the initial model, as the majority of remaining *mpeg1*-expressing cells in the *csf1ra*$^{-/-}$ line
502 correspond to DC-like cells, and not adult microglia. Notably, these results are consistent with the
503 reported loss of *ccl34b.1*$^{+}$; *mpeg1*$^{+}$ cells in *csf1ra*$^{-/-}$ fish by Wu and colleagues (Wu et al. 2020), and with
504 the observed upregulation of DC-like genes coupled to a downregulation of microglia markers in
505 *mpeg1*:GFP cells isolated from the brain of *csf1ra*$^{-/-}$ *csf1rb*$^{+/-}$ mutant animals (Oosterhof et al. 2018).

506 In zebrafish little is known regarding lymphoid cells in the adult CNS. Similar to DCs, lymphocytes are
507 present in limited numbers in the healthy mammalian brain and mainly restricted to the meningeal layers,
508 choroid plexus or the perivascular space (Mundt et al. 2019; Croese, Castellani, and Schwartz 2021). In
509 our transcriptomic analysis, we identified an heterogenous repertoire of lymphoid cells: T, NK and ILCs. B
510 lymphocytes, which could not be captured using the *cd45:DsRed* transgene (Wittamer et al. 2011), were
511 also detected using the *IgM*:GFP line, albeit in very low numbers. Our data suggest that, similar to
512 mammals, in zebrafish lymphoid cells in the steady-state are only occasionally found in the brain
513 parenchyma, and are most likely localized in the brain border regions. Here, it is worth noting that our
514 protocol for brain dissection requires the removal of the skull, which may completely or partially disrupt
515 the thin meningeal layers. Consequently, whether non parenchymal cells identified in this study are
516 located in the meninges, in the choroid plexus or even in the blood circulation remains to be determined.

517 Although the innate counterparts of the lymphoid system (NK cells and ILCs) have been identified in
518 different zebrafish organs (Hernández 2018; Silva et al. 2021; Tang et al. 2017), the lack of specific
519 fluorescent reporter lines has until now precluded a detailed characterization of these cell populations. In
520 particular, as a recently discovered cell type in zebrafish (Hernández 2018), the phenotypic and functional
521 heterogeneity of ILC-like cells are still poorly understood. In this study, we found that the adult zebrafish
522 brain contains a population that resembles the ILC2 subset in mammals. Like human and mouse ILC2s,
523 these cells do not express the T cell receptor *cd4-1*. However, these cells are positive for T_H2 cytokines
524 *il13* and *il4*, and also express *gata3*, a transcription factor involved in ILC2 differentiation. Surprisingly, *lck*
525 expression in our dataset was restricted to T lymphocytes and NK cells, whereas as in humans this gene is
526 also expressed in all ILCs (Bjorklund et al. 2016). A previous study in zebrafish reported populations
527 representing all three ILC subtypes isolated from the intestine based on expression of the *lck:GFP*
528 transgene (Hernández 2018). That suggests a conserved *lck* expression pattern across species. However,
529 in none of these experiments the presence of ILCs in the *lck:GFP* negative fraction was investigated, so
530 whether the absence of *lck* transcripts in our ILC2 dataset is due to a low detection sensitivity or a lack of
531 expression remains an open question. Nevertheless, as we showed, the level of expression of ILC2
532 transcripts remain specifically unchanged in brain leukocytes in the context of T cell deficiency. This
533 validates that ILC2 are indeed present in this organ. In line with this, innate-lymphoid-like cells
534 differentially expressing *il4*, *il13* and *gata3* have been recently annotated in the juvenile zebrafish brain
535 (Silva et al. 2021).

536 To conclude, our study provides a single-cell transcriptomic dataset of different brain leukocyte
537 populations, and may serve as a reference to better characterize the immune cell complexity of the
538 zebrafish brain in the steady state. Similar to mammalian microglia, zebrafish microglia are identified

539 based on several common canonical markers, some of which are conserved between species, but their
540 diversity is still poorly understood. Therefore, future investigations will benefit from mapping microglia
541 heterogeneity across the zebrafish brain as a complementary approach to single-cell transcriptomics for
542 studying microglia functions in health and disease. Further work will also be needed to elucidate the
543 functions of some of the cell types identified in this study, especially DC-like cells, and to elucidate whether
544 this population maintains locally or is continually replenished by cells from the periphery.

545

546 **MATERIALS AND METHODS**

547 **Zebrafish husbandry**

548 Zebrafish were maintained under standard conditions, according to FELASA (Alestrom et al. 2019) and
549 institutional (Université Libre de Bruxelles, Brussels, Belgium; ULB) guidelines and regulations. All
550 experimental procedures were approved by the ULB ethical committee for animal welfare (CEBEA) from
551 the ULB. The following lines were used: *Tg(mhc2dab:GFP$_{LT}$)^{sd67}* (Wittamer et al. 2011),
552 *Tg(ptprc:DsRed^{express})^{sd3}* (here referred to as *cd45:DsRed*) (Wittamer et al. 2011), *Tg(mpeg1.1:eGFP)^{gl22}*
553 (here referred to as *mpeg1:GFP*) (Ellett et al. 2010), *Tg(mpeg1.1:mCherry)^{gl23}* (here referred to as
554 *mpeg1:mCherry*) (Ellett et al. 2010), *TgBAC(p2ry12:p2ry12-GFP)^{hdb3}* (Sieger et al. 2012), *Tg(lck:lck-eGFP)^{cz1}*
555 (here referred to as *lck:GFP*) (Langenau et al. 2004), *TgBAC(cd4-1:mcherry)^{UMC13}* (here referred to as *cd4-*
556 *1:mCherry*) (Dee et al. 2016), *Tg(Cau.Ighv-ighm:EGFP)^{sd19}* (here referred to as *ighm:GFP*) (Page et al. 2013),
557 *Tg(mpx:GFP)^{i113}* (Mathias, Walters, and Huttenlocher 2009). The mutant lines used were: *panther^{i4e1}* (here
558 called *csf1ra$^{-/-}$*)(Parichy DM 2000); *csf1rb^{sa1503}*, generated via ethyl-nitrosurea (ENU) mutagenesis, were
559 obtained from the Sanger Institute Zebrafish Mutation Project and previously characterized (Ferrero et al.
560 2021), *irf8^{std96}* (Shiau et al. 2015), *rag2^{E450fs}* (Tang et al. 2014). Special care was taken to control reporter
561 gene dosage through experiments (with all control and mutant animals used in this study known to carry
562 similar hemizygous or homozygous doses of the GFP transgenes). The term "adult" fish refers to animals
563 aged between 4 months and 8 months old. For clarity, throughout the text, transgenic animals are
564 referred to without allele designations.

565

566 **Generation of *batf3$^{-/-}$* mutant zebrafish**

567 The *batf3* (ENSDARG00000042577) knockout mutant line was generated using the CRISPR/Cas9 system.
568 A single guide RNA (sgRNA) targeting the ATG start in the first exon (targeting sequence:
569 GAAGTGATGCTCCAGCTCTA) was identified and selected for its highest on-target activity and lowest
570 predicted off-target score using a combination of the Sequence Scan for CRISPR software (available at
571 http://crispr.dfci.har- vard.edu/SSC/) (Xu et al. 2015) and the CRISPR Scan (available at
572 http://www.crisprscan.org/). The DNA template for the sgRNA synthesis was produced using the PCR-
573 based short-oligo method as described (Talbot and Amacher 2014). The following primers were used: Fw:
574 5'- GCGATTTAGGTGACACTATA-3' and Rv: 5'- AAAGCACCGACTCGGTGCCAC-3'. The resulting PCR product
575 was purified by phenol-chloroform extraction and used for *in vitro* transcription using SP6 RNA-
576 polymerase (NEB, M0207). The resulting sgRNA was purified using the High Pure PCR Cleanup Microkit
577 (Roche, 498395500). 60 pg sgRNA and 100 pg Cas9 protein (PNA Bio) were co-injected into one-cell stage
578 *wild-type* embryos. The genotyping of both embryos and adults was performed using the following
579 primers: *batf3* fw: 5'- ACTTGACAGTTTAAGCATGCCT-3' and *batf3* rv: 5'- GAACATACCTCGCTCTGTCG-3'.

580 PCR amplicons were analyzed using a heteroduplex mobility assay (on a 8% polyacrylamide gel) to assess
581 the presence of CRISPR/Cas9-induced mutations.

582 The *batf3*^{ulb31} line carries an 8-bp deletion in exon 1. The deletion introduces a frameshift after amino acid
583 16 of the predicted 121-amino acid ORF, followed by 8 heterologous amino acids and then three
584 successive premature stop codons. Heterozygous F1 fish were backcrossed at least four generations with
585 AB* *wild-types* before being crossed to *Tg(mhc2dab:GFP; cd45:DsRed)* fish, as well as *Tg(p2ry12:p2ry12-*
586 *GFP; mpeg1:mCherry)* animals for phenotype assessment.

587

588 **Flow cytometry and cell sorting**

589 Cell suspensions from adult brains were obtained as previously described (Wittamer et al. 2011; Ferrero
590 et al. 2021; Ferrero et al. 2018). Briefly, adult brains dissected in 0.9X Dulbecco's Phosphate Buffered
591 Saline (DPBS) were triturated and treated with Liberase TM at 33°C for 30-45 minutes, fully dissociated
592 using a syringe with a 26G needle and washed in 2% fetal bovine serum diluted in 0.9X DPBS. Cell
593 suspensions were centrifuged at 290g 4ºC 10 min and filtered through a 40µm nylon mesh. Just before
594 flow cytometry analysis, SYTOX^{TM}Red (Invitrogen) was added to the samples at a final concentration of
595 5nM to exclude non viable cells. Flow cytometry acquisition and cell sorting was performed on a FACS
596 ARIA II (Becton Dickinson). To perform the qPCR experiments, between 7,000-10,000 *cd45:DsRed+*
597 leukocytes and approximately 2,500 *p2ry12:GFP*$^{+}$*; mpeg1:mCherry*$^{+}$ microglia or *p2ry12:GFP*$^{-}$*;*
598 *mpeg1:mCherry*$^{+}$ DC-like cells were sorted, collected in RLT Plus buffer (Qiagen) and flash freezed in liquid
599 nitrogen. Analyses were performed using FlowJo software. For morphological evaluation, 100,000
600 *cd45*:DsRed^{+} sorted cells were concentrated by cytocentrifugation at 300g for 10 minutes onto glass slides
601 using a Cellspin (Tharmac). Slides were air-dried, fixed with methanol for 5 minutes and stained with May-
602 Grünwald solution (Sigma) for 10 minutes. Then, slides were stained with a 1:5 dilution of Giemsa solution
603 (Sigma) in distilled water (dH_2O) for 20 minutes, rinsed in dH_2O, dehydrated through ethanol series and
604 mounted with DPX (Sigma).

605

606 **Bulk RNA sequencing and data analysis**

607 **Sample processing and cDNA.** Cell sorting and RNA sequencing was performed as previously described
608 (Kuil et al. 2020). Approximately 8,000 microglial cells (*p2ry12*$^{+}$*; cd45*$^{+}$ or *mhc2dab*$^{+}$*; cd45*^{low}, n=2 for each
609 Tg) and 1,200 DC-like cells (*mhc2dab*$^{+}$*; cd45*^{high}, n=2) were sorted. RNA was isolated using the miRNeasy
610 Micro Kit (Qiagen) according to the manufacturer's instructions. RNA concentration and quality were
611 evaluated using a Bioanalyzer 2100 (Agilent technologies). The Ovation Solo RNA-Seq System (NuGen-
612 TECAN) with the SoLo Custom AnyDeplete Probe Mix (Zebrafish probe set) were used to obtain indexed
613 cDNA libraries following manufacturer recommendation. **Sequencing.** Sequencing libraries were loaded
614 on a NovaSeq 6000 (Illumina) using a S2 flow cell and reads/fragments were sequenced using a 200 Cycle
615 Kit. **Alignment and feature counting.** Sequenced reads were then trimmed using *cutadapt* with default
616 parameters except for "--overlap 5 --cut 5 --minimum-length 25:25 -e 0.05". Trimmed FQ files were at this
617 point processed with the same approach for both datasets, including Wu et al. 2021 expression data that
618 were retrieved from GEO data repository (GEO Accession: GSM4725741) (Wu et al. 2020). Trimmed and
619 filtered reads were then mapped against the reference genome GRCz11.95 using STAR aligner with the "–
620 twopassMode basic" and "–sjdbOverhang 100". BAM files were then indexed and filtered using

621 SAMTOOLS "view -b -f 3 -F 256". Finally, transcript feature annotations for Ensembl genes using
622 *Danio_rerio* v. GRCz11.95 were quantified using HTSeq-counts call with default parameters specifying "-r
623 pos -s yes -a 10 --additional-attr=gene_name -m intersection-nonempty --secondary-alignments=ignore -
624 -supplementary-alignments=ignore". General sequencing and mapping stats were calculated using fastqc
625 and multiQC. **Feature count matrix preprocessing, normalization and differential expression.** Feature
626 count matrices were further preprocessed filtering low count genes (>=10#) for 2 out of 2 samples in each
627 group (this manuscript dataset) or 3 out of 5 samples per group (Wu et al. 2020 dataset). Overall, for this
628 manuscript dataset, we obtained 13663 genes expressed in both replicates whereas Wu et al. 2020
629 dataset, showed 9007 genes that were expressed in at least 3 of the 5 replicates. Then DESeq2 (v. 1.30.0)
630 for R statistical computing was used to normalize the raw counts and perform differential expression
631 analysis focussing on protein-coding genes with de-duplicated gene names (as "_#") (Love, Huber, and
632 Anders 2014). Statistical differential expression and downstream analyses were performed using R
633 Statistical software v. 4.0.3.

634

635 **Single-cell RNA sequencing and data analysis**

636 **Single-Cell RNA-seq library preparation and sequencing.** Adult brain single-cell suspensions were
637 prepared as described before from adult *Tg(p2ry12:GFP; cd45:DsRed)* fish (n=3), using calcein violet to
638 exclude dead cells (1µM, Thermo Fisher). A total of 14,000 *cd45:DsRed*$^{+}$ cells were processed for single-
639 cell profiling using the 10x Genomics platform and diluted to a density of 800 cells/µl following 10x
640 Genomics Chromium Single cell 3' kit (v3) instructions. Library preparation was performed according to
641 10x Genomics guidelines and sequenced on an Illumina NextSeq 550. Raw sequencing data was processed
642 using the Cell Ranger with a custom-built reference based on the zebrafish reference genome GRCz11 and
643 gene annotation Ensembl 92 in which the EGFP and DsRed sequence were included.

644 **Single-cell RNA-seq data preprocessing.** Single cell raw counts were processed using Seurat (v3)(Butler et
645 al. 2018; Satija et al. 2015). Briefly, genes with zero counts for all cells were removed, and applied cell
646 filters for >=20% reads mapping to mitochondrial genes and nFeature >300. Additionally, mitochondrial
647 genes '^mt-' and ribosomal genes '^rp[sl]' were masked for further downstream analysis, as well as non-
648 coding protein genes selected with the current feature annotations of the EnsemblGene 95 from GRCz11
649 zebrafish genome. Overall, providing a dataset of 4,145 cells and 18,807 genes for single cell data analysis.
650 **Single-Cell Normalization, clustering and marker genes.** Filtered cell data was normalized using the SCT
651 transform approach for Seurat using "variable.features.n=4000 and return.only.var.genes=F". Then, the
652 nearest neighbour graph was build with 40 PCA dimensions, and clusters were identified using manually
653 selected resolution based on the supervised inspection of know markers leading to the optimal
654 "resolution= 0.6 (Louvain)" and "n.neighbors=20". The same parameters were used for the dimensionality
655 reduction as UMAP. Finally, cluster annotation was performed by inspecting the identified marker genes
656 using FindAllMarkers function (one v. rest with default parameters except for "min.pct=0.25""". **Single Cell**
657 **Pathway analysis.** For pathway analysis, marker genes of all four microglia clusters together (MG1, MG2,
658 MG3, MG4) or all four DC-like clusters (DC1, DC2, DC3, DC4) were obtained using Seurat's FindMarkers
659 function. Next, differentially expressed zebrafish genes (log2 fold-change >0.25, P-adjusted < 0.05) were
660 converted to their human orthologs using gProfiler tool (Raudvere et al. 2019) and validated using the
661 ZFIN (zfin.org) and Alliance Genome databases (www.alliancegenome.org). Genes with no corresponding
662 orthologs were not included. From this gene lists, Gene ontology terms (Biological Processes) and

663 Reactome pathways were obtained using the Cytoscape ClueGO application (two-sided hypergeometric
664 statistical test, Bonferroni correction)(Bindea et al. 2009). To explore MG and DC-like conserved cell type
665 signatures (**Table 4**), each gene list was uploaded to the Enrichr databas (Xie et al. 2021) to identify the
666 most enriched "Cell Types" categories querying PanglaoDB (Franzen, Gan, and Bjorkegren 2019).

667

668 **Quantitative PCR**

669 RNA extraction was performed using the RNeasy Plus Mini kit (Qiagen) and cDNAs were synthesized using
670 the qscript cDNA supermix (Quanta Biosciences), as previously described (Ferrero et al. 2018). Reactions
671 were run on a Bio-Rad CFX96^{TM} real time system (Bio-Rad), using the Kapa SYBR Fast qPCR Master Mix
672 (2X) kit (Kapa Biosystems) under the following thermal cycling conditions: 3 min at 95°C and 40 cycles of
673 5 s at 95°C, 30 s at 60°C. A final dissociation at 95ºC for 10 s and a melting curve from 65 to 95°C (0.5°C
674 increase every 5 s) were included to verify the specificity and absence of primer dimers. Biological
675 replicates were compared for each subset. Relative amount of each transcript was quantified via the ΔCt
676 method, using *elongation-Factor-1-alpha* (*eef1a1l1*; ENSDARG00000020850) expression for
677 normalization.

678

679 **Immunostaining and vibratome sections**

680 Adult brains were dissected, fixed in 4% PFA, incubated overnight in 30% sucrose:PBS before snap-freezing
681 in OCT (Tissue-Tek, Leica) and stored at -80ºC. Immunostaining was performed on 14 µm cryosections as
682 described (Ferrero et al. 2018). The following primary and secondary antibodies were used: chicken anti-
683 GFP polyclonal antibody (1:500; Abcam, Cat# ab13970), rabbit anti-Lcp1 (1:1000), mouse anti-mCherry
684 monoclonal antibody (1:500; Takara Bio Cat# 632543), Alexa Fluor 488-conjugated anti-chicken IgG
685 antibody (1:500; Abcam Cat# ab150169), Alexa Fluor 594- conjugated anti-rabbit IgG (1:500; Abcam Cat#
686 ab150076), Alexa Fluor 647-conjugated anti-mouse IgG (1:500; Abcam Cat# ab150107). For vibratome
687 sections, adult brains were fixed in 4% PFA and included in 7% low-melting agarose in PBS 1X and
688 sectioned at 100 µm using a vibratome (Leica). Sections were mounted with Glycergel (Dako) and imaged.

689

690 **Imaging and image analyses**

691 Fluorescent samples were imaged using a Zeiss LSM 780 inverted microscope (Zeiss, Oberkochen,
692 Germany), with a Plan Apochromat 20X objective. Image post-processing was performed using Zeiss Zen
693 Software (ZEN Digital Imaging for Light Microscopy), as previously described (Ferrero et al. 2021). Cells
694 were manually counted using the Black Zen software and divided by the area of the brain section (cell
695 density/µm^2) and quantified between 5-11 transveral sections per brain. Cytospuned cells were imaged
696 using a Leica DM 2000 microscope equipped with a 100X objective, and scanned using a NanoZoomer-SQ
697 Digital Slide scanner (Hamamatsu).

698

699 **Data collection**

The sample size was chosen based on previous experience in the laboratory, for each experiment to yield high power to detect specific effects. No statistical methods were used to predetermine sample size and experiments were repeated at least twice. Homozygous mutant animals used in this study were obtained by heterozygous mating. No fish were excluded. Genotyping was performed on tail biopsies collected from individual euthanized fish, in parallel to brain dissection. Randomly selected samples for each genotype were then immunostained in one batch, assessed phenotypically in a blind manner and grouped based on their genotype.

Statistical analyses

Statistical differences between mean values of two experimental groups were analyzed by Student's t-test or the equivalent U-Mann-Whitney non-parametric test, when parametric assumptions were not met in the sample data. Results are expressed as mean ± standard of the mean (SEM) and considered to be significant at $P < 0.05$. Details on the number of fish (biological replicates) used in each experiment, the statistical test used and statistical significance are indicated in each figure and figure legends. Statistical analyses were performed using GraphPad Prism8.

ACKNOWLEDGEMENTS

We thank all members of the Wittamer lab and Sumeet Pal Singh for critical discussion and comments on the manuscript. We are also grateful to Marianne Caron for technical assistance and to Daniel M. Borràs for guidance with bioinformatic analyses. We also aknowledge Christine Dubois for support with flow cytometry, F. Libert and A. Lefort from the ULB Genomic Core Facility and S. Reinhardt, A. Kränkel and A. Petzold at the Dresden-Concept Genome center in Germany.

COMPETING INTERESTS

The authors declare no competing financial interests.

FUNDING

This work was funded in part by the Funds for Scientific Research (FNRS) under Grant Numbers F451218F, UN06119F and UG03019F, the program ARC from the Wallonia-Brussels Federation, the Minerve Foundation (to V.W.), the Fonds David et Alice Van Buuren, the Fondation Jaumotte-Demoulin and the Fondation Héger-Masson (to V.W. , G.F. and M.M.). M.R. is supported by a Chargé de Recherche fellowship (FNRS), G.F. and A.M. by a Research Fellowship (FNRS) and M.M. by a fellowship from The Belgian Kid's Fund.

DATA AVAILABILTY STATEMENT

All datasets and material generated for this study are included in the manuscript/ Supplementary Files and will be shared upon request. Raw data for single cell RNA-seq samples and RNA-seq are available in the ArrayExpress database as accession number E-MTAB-13223 and E-MTAB-13228, respectively.

REFERENCES

Alestrom, P., L. D'Angelo, P. J. Midtlyng, D. F. Schorderet, S. Schulte-Merker, F. Sohm, and S. Warner. 2019. 'Zebrafish: Housing and husbandry recommendations', *Lab Anim*: 23677219869037.

Alves de Lima, K., J. Rustenhoven, S. Da Mesquita, M. Wall, A. F. Salvador, I. Smirnov, G. Martelossi Cebinelli, T. Mamuladze, W. Baker, Z. Papadopoulos, M. B. Lopes, W. S. Cao, X. S. Xie, J. Herz, and J. Kipnis. 2020. 'Meningeal gammadelta T cells regulate anxiety-like behavior via IL-17a signaling in neurons', *Nat Immunol*, 21: 1421-29.

Bassity, E., and T. G. Clark. 2012. 'Functional identification of dendritic cells in the teleost model, rainbow trout (Oncorhynchus mykiss)', *PLoS One*, 7: e33196.

Bindea, G., B. Mlecnik, H. Hackl, P. Charoentong, M. Tosolini, A. Kirilovsky, W. H. Fridman, F. Pages, Z. Trajanoski, and J. Galon. 2009. 'ClueGO: a Cytoscape plug-in to decipher functionally grouped gene ontology and pathway annotation networks', *Bioinformatics*, 25: 1091-3.

Bjorklund, A. K., M. Forkel, S. Picelli, V. Konya, J. Theorell, D. Friberg, R. Sandberg, and J. Mjosberg. 2016. 'The heterogeneity of human CD127(+) innate lymphoid cells revealed by single-cell RNA sequencing', *Nat Immunol*, 17: 451-60.

Bottcher, C., S. Schlickeiser, M. A. M. Sneeboer, D. Kunkel, A. Knop, E. Paza, P. Fidzinski, L. Kraus, G. J. L. Snijders, R. S. Kahn, A. R. Schulz, H. E. Mei, N. B. B. Psy, E. M. Hol, B. Siegmund, R. Glauben, E. J. Spruth, L. D. de Witte, and J. Priller. 2019. 'Human microglia regional heterogeneity and phenotypes determined by multiplexed single-cell mass cytometry', *Nat Neurosci*, 22: 78-90.

Butler, A., P. Hoffman, P. Smibert, E. Papalexi, and R. Satija. 2018. 'Integrating single-cell transcriptomic data across different conditions, technologies, and species', *Nat Biotechnol*, 36: 411-20.

Butovsky, O., M. P. Jedrychowski, C. S. Moore, R. Cialic, A. J. Lanser, G. Gabriely, T. Koeglsperger, B. Dake, P. M. Wu, C. E. Doykan, Z. Fanek, L. Liu, Z. Chen, J. D. Rothstein, R. M. Ransohoff, S. P. Gygi, J. P. Antel, and H. L. Weiner. 2014. 'Identification of a unique TGF-beta-dependent molecular and functional signature in microglia', *Nat Neurosci*, 17: 131-43.

Butovsky, O., and H. L. Weiner. 2018. 'Microglial signatures and their role in health and disease', *Nat Rev Neurosci*, 19: 622-35.

Cabeza-Cabrerizo, M., A. Cardoso, C. M. Minutti, M. Pereira da Costa, and E. Sousa C. Reis. 2021. 'Dendritic Cells Revisited', *Annu Rev Immunol*, 39: 131-66.

Carmona, S. J., S. A. Teichmann, L. Ferreira, I. C. Macaulay, M. J. Stubbington, A. Cvejic, and D. Gfeller. 2017. 'Single-cell transcriptome analysis of fish immune cells provides insight into the evolution of vertebrate immune cell types', *Genome Res*, 27: 451-61.

Croese, T., G. Castellani, and M. Schwartz. 2021. 'Immune cell compartmentalization for brain surveillance and protection', *Nat Immunol*, 22: 1083-92.

D'Amora, M., A. Galgani, M. Marchese, F. Tantussi, U. Faraguna, F. De Angelis, and F. S. Giorgi. 2023. 'Zebrafish as an Innovative Tool for Epilepsy Modeling: State of the Art and Potential Future Directions', *Int J Mol Sci*, 24.

Dee, C. T., R. T. Nagaraju, E. I. Athanasiadis, C. Gray, L. Fernandez Del Ama, S. A. Johnston, C. J. Secombes, A. Cvejic, and A. F. Hurlstone. 2016. 'CD4-Transgenic Zebrafish Reveal Tissue-Resident Th2- and Regulatory T Cell-like Populations and Diverse Mononuclear Phagocytes', *J Immunol*, 197: 3520-30.

781 Drieu, A., S. Du, S. E. Storck, J. Rustenhoven, Z. Papadopoulos, T. Dykstra, F. Zhong, K. Kim, S. Blackburn,
782 T. Mamuladze, O. Harari, C. M. Karch, R. J. Bateman, R. Perrin, M. Farlow, J. Chhatwal, Network
783 Dominantly Inherited Alzheimer, S. Hu, G. J. Randolph, I. Smirnov, and J. Kipnis. 2022.
784 'Parenchymal border macrophages regulate the flow dynamics of the cerebrospinal fluid', *Nature*,
785 611: 585-93.
786 Earley, A. M., C. L. Graves, and C. E. Shiau. 2018. 'Critical Role for a Subset of Intestinal Macrophages in
787 Shaping Gut Microbiota in Adult Zebrafish', *Cell Rep*, 25: 424-36.
788 Ellett, F., L. Pase, J. W. Hayman, A. Andrianopoulos, and G. J. Lieschke. 2010. 'mpeg1 promoter transgenes
789 direct macrophage-lineage expression in zebrafish', *Blood*, 117: e49-56.
790 Ferrero, G., E. Gomez, S. Lyer, M. Rovira, M. Miserocchi, D. M. Langenau, J. Y. Bertrand, and V. Wittamer.
791 2020. 'The macrophage-expressed gene (mpeg) 1 identifies a subpopulation of B cells in the adult
792 zebrafish', *J Leukoc Biol*, 107: 431-43.
793 Ferrero, G., C. B. Mahony, E. Dupuis, L. Yvernogeau, E. Di Ruggiero, M. Miserocchi, M. Caron, C. Robin, D.
794 Traver, J. Y. Bertrand, and V. Wittamer. 2018. 'Embryonic Microglia Derive from Primitive
795 Macrophages and Are Replaced by cmyb-Dependent Definitive Microglia in Zebrafish', *Cell Rep*,
796 24: 130-41.
797 Ferrero, G., M. Miserocchi, E. Di Ruggiero, and V. Wittamer. 2021. 'A csf1rb mutation uncouples two waves
798 of microglia development in zebrafish', *Development*.
799 Franzen, O., L. M. Gan, and J. L. M. Bjorkegren. 2019. 'PanglaoDB: a web server for exploration of mouse
800 and human single-cell RNA sequencing data', *Database (Oxford)*, 2019.
801 Gerrits, E., Y. Heng, Ewgm Boddeke, and B. J. L. Eggen. 2020. 'Transcriptional profiling of microglia; current
802 state of the art and future perspectives', *Glia*, 68: 740-55.
803 Hammond, T. R., C. Dufort, L. Dissing-Olesen, S. Giera, A. Young, A. Wysoker, A. J. Walker, F. Gergits, M.
804 Segel, J. Nemesh, S. E. Marsh, A. Saunders, E. Macosko, F. Ginhoux, J. Chen, R. J. M. Franklin, X.
805 Piao, S. A. McCarroll, and B. Stevens. 2018. 'Single-Cell RNA Sequencing of Microglia throughout
806 the Mouse Lifespan and in the Injured Brain Reveals Complex Cell-State Changes', *Immunity*.
807 Hason, M., T. Mikulasova, O. Machonova, A. Pombinho, T. J. van Ham, U. Irion, C. Nusslein-Volhard, P.
808 Bartunek, and O. Svoboda. 2022. 'M-CSFR/CSF1R signaling regulates myeloid fates in zebrafish via
809 distinct action of its receptors and ligands', *Blood Adv*, 6: 1474-88.
810 Herbomel, P., B. Thisse, and C. Thisse. 2001. 'Zebrafish early macrophages colonize cephalic mesenchyme
811 and developing brain, retina, and epidermis through a M-CSF receptor-dependent invasive
812 process', *Dev Biol*, 238: 274-88.
813 Hernández, P. P.; Strzelecka, P. M.; Athanasiadis, E. I.; Dominic Hall. D.; Robalo. A. F.; Collins, C. M.;
814 Boudinot, P.; Levraud, J. P.; Cvejic, A. 2018. 'Single-cell transcriptional analysis reveals ILC-like cells
815 in zebrafish', *Sci. Immunol.*, 3.
816 Jordao, M. J. C., R. Sankowski, S. M. Brendecke, Sagar, G. Locatelli, Y. H. Tai, T. L. Tay, E. Schramm, S.
817 Armbruster, N. Hagemeyer, O. Gross, D. Mai, O. Cicek, T. Falk, M. Kerschensteiner, D. Grun, and
818 M. Prinz. 2019. 'Single-cell profiling identifies myeloid cell subsets with distinct fates during
819 neuroinflammation', *Science*, 363.
820 Jurga, A. M., M. Paleczna, and K. Z. Kuter. 2020. 'Overview of General and Discriminating Markers of
821 Differential Microglia Phenotypes', *Front Cell Neurosci*, 14: 198.
822 Kaunzner, U. W., M. M. Miller, A. Gottfried-Blackmore, J. Gal-Toth, J. C. Felger, B. S. McEwen, and K.
823 Bulloch. 2012. 'Accumulation of resident and peripheral dendritic cells in the aging CNS', *Neurobiol*
824 *Aging*, 33: 681-93 e1.
825 Kizil, C., N. Kyritsis, S. Dudczig, V. Kroehne, D. Freudenreich, J. Kaslin, and M. Brand. 2012. 'Regenerative
826 neurogenesis from neural progenitor cells requires injury-induced expression of Gata3', *Dev Cell*,
827 23: 1230-7.

828 Kuil, L. E., N. Oosterhof, G. Ferrero, T. Mikulasova, M. Hason, J. Dekker, M. Rovira, H. C. van der Linde, P.
829 M. van Strien, E. de Pater, G. Schaaf, E. M. Bindels, V. Wittamer, and T. J. van Ham. 2020. 'Zebrafish
830 macrophage developmental arrest underlies depletion of microglia and reveals Csf1r-
831 independent metaphocytes', *Elife*, 9.
832 Kuil, L. E., N. Oosterhof, S. N. Geurts, H. C. van der Linde, E. Meijering, and T. J. van Ham. 2019. 'Reverse
833 genetic screen reveals that Il34 facilitates yolk sac macrophage distribution and seeding of the
834 brain', *Dis Model Mech*, 12.
835 Kyritsis, N., C. Kizil, S. Zocher, V. Kroehne, J. Kaslin, D. Freudenreich, A. Iltzsche, and M. Brand. 2012. 'Acute
836 inflammation initiates the regenerative response in the adult zebrafish brain', *Science*, 338: 1353-
837 6.
838 Langenau, D. M., A. A. Ferrando, D. Traver, J. L. Kutok, J. P. Hezel, J. P. Kanki, L. I. Zon, A. T. Look, and N. S.
839 Trede. 2004. 'In vivo tracking of T cell development, ablation, and engraftment in transgenic
840 zebrafish', *Proc Natl Acad Sci U S A*, 101: 7369-74.
841 Lewis, K. L., N. Del Cid, and D. Traver. 2014. 'Perspectives on antigen presenting cells in zebrafish', *Dev*
842 *Comp Immunol*, 46: 63-73.
843 Liu, Y. 2023. 'Zebrafish as a Model Organism for Studying Pathologic Mechanisms of Neurodegenerative
844 Diseases and other Neural Disorders', *Cell Mol Neurobiol*, 43: 2603-20.
845 Love, M. I., W. Huber, and S. Anders. 2014. 'Moderated estimation of fold change and dispersion for RNA-
846 seq data with DESeq2', *Genome Biol*, 15: 550.
847 Ludewig, P., M. Gallizioli, X. Urra, S. Behr, V. H. Brait, M. Gelderblom, T. Magnus, and A. M. Planas. 2016.
848 'Dendritic cells in brain diseases', *Biochim Biophys Acta*, 1862: 352-67.
849 Lugo-Villarino, G., K. M. Balla, D. L. Stachura, K. Banuelos, M. B. Werneck, and D. Traver. 2010.
850 'Identification of dendritic antigen-presenting cells in the zebrafish', *Proc Natl Acad Sci U S A*, 107:
851 15850-5.
852 Maddaluno, L., S. E. Verbrugge, C. Martinoli, G. Matteoli, A. Chiavelli, Y. Zeng, E. D. Williams, M. Rescigno,
853 and U. Cavallaro. 2009. 'The adhesion molecule L1 regulates transendothelial migration and
854 trafficking of dendritic cells', *J Exp Med*, 206: 623-35.
855 Masuda, T., R. Sankowski, O. Staszewski, C. Bottcher, L. Amann, C. Scheiwe, S. Nessler, P. Kunz, G. van Loo,
856 V. A. Coenen, P. C. Reinacher, A. Michel, U. Sure, R. Gold, J. Priller, C. Stadelmann, and M. Prinz.
857 2019. 'Spatial and temporal heterogeneity of mouse and human microglia at single-cell
858 resolution', *Nature*, 566: 388-92.
859 Masuda, Takahiro, Roman Sankowski, Ori Staszewski, and Marco Prinz. 2020. 'Microglia Heterogeneity in
860 the Single-Cell Era', *Cell Reports*, 30: 1271-81.
861 Mathias, J. R., K. B. Walters, and A. Huttenlocher. 2009. 'Neutrophil motility in vivo using zebrafish',
862 *Methods Mol Biol*, 571: 151-66.
863 Mazzolini, J., S. Le Clerc, G. Morisse, C. Coulonges, L. E. Kuil, T. J. van Ham, J. F. Zagury, and D. Sieger. 2019.
864 'Gene expression profiling reveals a conserved microglia signature in larval zebrafish', *Glia*.
865 Milner, J. J., C. Toma, B. Yu, K. Zhang, K. Omilusik, A. T. Phan, D. Wang, A. J. Getzler, T. Nguyen, S. Crotty,
866 W. Wang, M. E. Pipkin, and A. W. Goldrath. 2017. 'Runx3 programs CD8(+) T cell residency in non-
867 lymphoid tissues and tumours', *Nature*, 552: 253-57.
868 Minhas, Paras S., Amira Latif-Hernandez, Melanie R. McReynolds, Aarooran S. Durairaj, Qian Wang,
869 Amanda Rubin, Amit U. Joshi, Joy Q. He, Esha Gauba, Ling Liu, Congcong Wang, Miles Linde, Yuki
870 Sugiura, Peter K. Moon, Ravi Majeti, Makoto Suematsu, Daria Mochly-Rosen, Irving L. Weissman,
871 Frank M. Longo, Joshua D. Rabinowitz, and Katrin I. Andreasson. 2021. 'Restoring metabolism of
872 myeloid cells reverses cognitive decline in ageing', *Nature*.
873 Moore, F. E., E. G. Garcia, R. Lobbardi, E. Jain, Q. Tang, J. C. Moore, M. Cortes, A. Molodtsov, M. Kasheta,
874 C. C. Luo, A. J. Garcia, R. Mylvaganam, J. A. Yoder, J. S. Blackburn, R. I. Sadreyev, C. J. Ceol, T. E.

875 North, and D. M. Langenau. 2016. 'Single-cell transcriptional analysis of normal, aberrant, and
876 malignant hematopoiesis in zebrafish', *J Exp Med*, 213: 979-92.
877 Moyse, B. R., and R. J. Richardson. 2020. 'A Population of Injury-Responsive Lymphoid Cells Expresses
878 mpeg1.1 in the Adult Zebrafish Heart', *Immunohorizons*, 4: 464-74.
879 Mrdjen, D., A. Pavlovic, F. J. Hartmann, B. Schreiner, S. G. Utz, B. P. Leung, I. Lelios, F. L. Heppner, J. Kipnis,
880 D. Merkler, M. Greter, and B. Becher. 2018. 'High-Dimensional Single-Cell Mapping of Central
881 Nervous System Immune Cells Reveals Distinct Myeloid Subsets in Health, Aging, and Disease',
882 *Immunity*, 48: 380-95 e6.
883 Mundt, S., M. Greter, A. Flugel, and B. Becher. 2019. 'The CNS Immune Landscape from the Viewpoint of
884 a T Cell', *Trends Neurosci*, 42: 667-79.
885 Oosterhof, N., L. E. Kuil, H. C. van der Linde, S. M. Burm, W. Berdowski, W. F. J. van Ijcken, J. C. van Swieten,
886 E. M. Hol, M. H. G. Verheijen, and T. J. van Ham. 2018. 'Colony-Stimulating Factor 1 Receptor
887 (CSF1R) Regulates Microglia Density and Distribution, but Not Microglia Differentiation In Vivo',
888 *Cell Rep*, 24: 1203-17 e6.
889 Page, D. M., V. Wittamer, J. Y. Bertrand, K. L. Lewis, D. N. Pratt, N. Delgado, S. E. Schale, C. McGue, B. H.
890 Jacobsen, A. Doty, Y. Pao, H. Yang, N. C. Chi, B. G. Magor, and D. Traver. 2013. 'An evolutionarily
891 conserved program of B-cell development and activation in zebrafish', *Blood*, 122: e1-11.
892 Parichy DM, Ransom DG, Paw B, Zon LI, Johnson SL. 2000. 'An orthologue of the kit-related gene fms is
893 required for development of neural crest-derived xanthophores and a subpopulation of adult
894 melanocytes in the zebrafish, Danio rerio.', *Development*, 127: 3031-44.
895 Pasciuto, E., O. T. Burton, C. P. Roca, V. Lagou, W. D. Rajan, T. Theys, R. Mancuso, R. Y. Tito, L. Kouser, Z.
896 Callaerts-Vegh, A. G. de la Fuente, T. Prezzemolo, L. G. Mascali, A. Brajic, C. E. Whyte, L. Yshii, A.
897 Martinez-Muriana, M. Naughton, A. Young et al. 2020. 'Microglia Require CD4 T Cells to Complete
898 the Fetal-to-Adult Transition', *Cell*, 182: 625-40 e24.
899 Peri, F., and C. Nusslein-Volhard. 2008. 'Live imaging of neuronal degradation by microglia reveals a role
900 for v0-ATPase a1 in phagosomal fusion in vivo', *Cell*, 133: 916-27.
901 Raudvere, U., L. Kolberg, I. Kuzmin, T. Arak, P. Adler, H. Peterson, and J. Vilo. 2019. 'g:Profiler: a web server
902 for functional enrichment analysis and conversions of gene lists (2019 update)', *Nucleic Acids Res*,
903 47: W191-W98.
904 Rovira, M., M. Miserocchi, A. Montanari, L. Hammou, L. Chomette, J. Pozo, V. Imbault, X. Bisteau, and V.
905 Wittamer. 2022. 'Zebrafish Galectin 3 binding protein is the target antigen of the microglial 4C4
906 monoclonal antibody', *Dev Dyn*.
907 Saraswathy, V. M., L. Zhou, A. R. McAdow, B. Burris, D. Dogra, S. Reischauer, and M. H. Mokalled. 2022.
908 'Myostatin is a negative regulator of adult neurogenesis after spinal cord injury in zebrafish', *Cell*
909 *Rep*, 41: 111705.
910 Satija, R., J. A. Farrell, D. Gennert, A. F. Schier, and A. Regev. 2015. 'Spatial reconstruction of single-cell
911 gene expression data', *Nat Biotechnol*, 33: 495-502.
912 Shiau, C. E., Z. Kaufman, A. M. Meireles, and W. S. Talbot. 2015. 'Differential requirement for irf8 in
913 formation of embryonic and adult macrophages in zebrafish', *PLoS One*, 10: e0117513.
914 Sieger, D., C. Moritz, T. Ziegenhals, S. Prykhozhij, and F. Peri. 2012. 'Long-range Ca2+ waves transmit brain-
915 damage signals to microglia', *Dev Cell*, 22: 1138-48.
916 Silva, N. J., L. C. Dorman, I. D. Vainchtein, N. C. Horneck, and A. V. Molofsky. 2021. 'In situ and
917 transcriptomic identification of microglia in synapse-rich regions of the developing zebrafish
918 brain', *Nat Commun*, 12: 5916.
919 Spits, H., and T. Cupedo. 2012. 'Innate lymphoid cells: emerging insights in development, lineage
920 relationships, and function', *Annu Rev Immunol*, 30: 647-75.
921 Stratoulias, V., J. L. Venero, M. E. Tremblay, and B. Joseph. 2019. 'Microglial subtypes: diversity within the
922 microglial community', *EMBO J*: e101997.

923 Talbot, J. C., and S. L. Amacher. 2014. 'A streamlined CRISPR pipeline to reliably generate zebrafish
924 frameshifting alleles', *Zebrafish*, 11: 583-5.
925 Tanabe, S., and T. Yamashita. 2018. 'B-1a lymphocytes promote oligodendrogenesis during brain
926 development', *Nat Neurosci*, 21: 506-16.
927 Tang, Q., N. S. Abdelfattah, J. S. Blackburn, J. C. Moore, S. A. Martinez, F. E. Moore, R. Lobbardi, I. M.
928 Tenente, M. S. Ignatius, J. N. Berman, R. S. Liwski, Y. Houvras, and D. M. Langenau. 2014.
929 'Optimized cell transplantation using adult rag2 mutant zebrafish', *Nat Methods*, 11: 821-4.
930 Tang, Q., S. Iyer, R. Lobbardi, J. C. Moore, H. Chen, C. Lareau, C. Hebert, M. L. Shaw, C. Neftel, M. L. Suva,
931 C. J. Ceol, A. Bernards, M. Aryee, L. Pinello, I. A. Drummond, and D. M. Langenau. 2017. 'Dissecting
932 hematopoietic and renal cell heterogeneity in adult zebrafish at single-cell resolution using RNA
933 sequencing', *J Exp Med*, 214: 2875-87.
934 Turrini, L., L. Roschi, G. de Vito, F. S. Pavone, and F. Vanzi. 2023. 'Imaging Approaches to Investigate
935 Pathophysiological Mechanisms of Brain Disease in Zebrafish', *Int J Mol Sci*, 24.
936 Van Hove, H., L. Martens, I. Scheyltjens, K. De Vlaminck, A. R. Pombo Antunes, S. De Prijck, N. Vandamme,
937 S. De Schepper, G. Van Isterdael, C. L. Scott, J. Aerts, G. Berx, G. E. Boeckxstaens, R. E.
938 Vandenbroucke, L. Vereecke, D. Moechars, M. Guilliams, J. A. Van Ginderachter, Y. Saeys, and K.
939 Movahedi. 2019. 'A single-cell atlas of mouse brain macrophages reveals unique transcriptional
940 identities shaped by ontogeny and tissue environment', *Nat Neurosci*, 22: 1021-35.
941 Vivier, E., D. Artis, M. Colonna, A. Diefenbach, J. P. Di Santo, G. Eberl, S. Koyasu, R. M. Locksley, A. N. J.
942 McKenzie, R. E. Mebius, F. Powrie, and H. Spits. 2018. 'Innate Lymphoid Cells: 10 Years On', *Cell*,
943 174: 1054-66.
944 Vivier, E., S. A. van de Pavert, M. D. Cooper, and G. T. Belz. 2016. 'The evolution of innate lymphoid cells',
945 *Nat Immunol*, 17: 790-4.
946 Wittamer, V., J. Y. Bertrand, P. W. Gutschow, and D. Traver. 2011. 'Characterization of the mononuclear
947 phagocyte system in zebrafish', *Blood*, 117: 7126-35.
948 Wong, S. H., J. A. Walker, H. E. Jolin, L. F. Drynan, E. Hams, A. Camelo, J. L. Barlow, D. R. Neill, V. Panova,
949 U. Koch, F. Radtke, C. S. Hardman, Y. Y. Hwang, P. G. Fallon, and A. N. McKenzie. 2012.
950 'Transcription factor RORalpha is critical for nuocyte development', *Nat Immunol*, 13: 229-36.
951 Wu, S. , L. T. M. Nguyen, H. Pan, S. Hassan, Y. Dai, J. Xu, and Z. Wen. 2020. 'Two phenotypically and
952 functionally distinct microglial populations in adult zebrafish', *Science Advances*.
953 Wu, S. Y., J. Shin, D. S. Sepich, and L. Solnica-Krezel. 2012. 'Chemokine GPCR signaling inhibits beta-catenin
954 during zebrafish axis formation', *PLoS Biol*, 10: e1001403.
955 Xie, Z., A. Bailey, M. V. Kuleshov, D. J. B. Clarke, J. E. Evangelista, S. L. Jenkins, A. Lachmann, M. L.
956 Wojciechowicz, E. Kropiwnicki, K. M. Jagodnik, M. Jeon, and A. Ma'ayan. 2021. 'Gene Set
957 Knowledge Discovery with Enrichr', *Curr Protoc*, 1: e90.
958 Xu, H., T. Xiao, C. H. Chen, W. Li, C. A. Meyer, Q. Wu, D. Wu, L. Cong, F. Zhang, J. S. Liu, M. Brown, and X.
959 S. Liu. 2015. 'Sequence determinants of improved CRISPR sgRNA design', *Genome Res*, 25: 1147-
960 57.
961 Yanez, A., and H. S. Goodridge. 2016. 'Interferon regulatory factor 8 and the regulation of neutrophil,
962 monocyte, and dendritic cell production', *Curr Opin Hematol*, 23: 11-7.
963 Yoder, J. A., P. M. Turner, P. D. Wright, V. Wittamer, J. Y. Bertrand, D. Traver, and G. W. Litman. 2010.
964 'Developmental and tissue-specific expression of NITRs', *Immunogenetics*, 62: 117-22.
965 Zambusi, A., K. T. Novoselc, S. Hutten, S. Kalpazidou, C. Koupourtidou, R. Schieweck, S. Aschenbroich, L.
966 Silva, A. S. Yazgili, F. van Bebber, B. Schmid, G. Moller, C. Tritscher, C. Stigloher, C. Delbridge, S.
967 Sirko, Z. I. Gunes, S. Liebscher, J. Schlegel et al. 2022. 'TDP-43 condensates and lipid droplets
968 regulate the reactivity of microglia and regeneration after traumatic brain injury', *Nat Neurosci*,
969 25: 1608-25.

970

Reagent type (species) or resource	Designation	Source or reference	Identifiers	Additional information
Genetic reagent (*Danio rerio*)	*Tg(mhc2dab:GFP$_{LT}$)^{sd67}*	(Wittamer et al. 2011)	ZFIN: *sd67*	
Genetic reagent (*Danio rerio*)	*Tg(ptprc:DsRed^{express})^{sd3}*	(Wittamer et al. 2011)	ZFIN: *sd3*	
Genetic reagent (*Danio rerio*)	*Tg(mpeg1.1:eGFP)^{gl22}*	(Ellett et al. 2010)	ZFIN: *gl22*	
Genetic reagent (*Danio rerio*)	*Tg(mpeg1.1:mCherry)^{gl23}*	(Ellett et al. 2010)	ZFIN: *gl23*	
Genetic reagent (*Danio rerio*)	*TgBAC(p2ry12:p2ry12-GFP)^{hdb3}*	(Sieger et al. 2012)	ZFIN: *hdb3*	
Genetic reagent (*Danio rerio*)	*Tg(lck:lck-eGFP)^{cz1}*	(Langenau et al. 2004)	ZFIN: *cz1*	
Genetic reagent (*Danio rerio*)	*TgBAC(cd4-1:mcherry)^{UMC13}*	(Dee et al. 2016)	ZFIN: *UMC13*	
Genetic reagent (*Danio rerio*)	*Tg(Cau.Ighv-ighm:EGFP)^{sd19}*	(Page et al. 2013)	ZFIN: *sd19*	
Genetic reagent (*Danio rerio*)	*Tg(mpx:GFP)^{i113}*	(Mathias, Walters, and Huttenlocher 2009)	ZFIN: *i113*	
Genetic reagent (*Danio rerio*)	*panther^{j4e1}*	(Parichy DM 2000)	ZFIN: *i4e1*	
Genetic reagent (*Danio rerio*)	*csf1rb^{sa1503}*	Sanger Institute Zebrafish Mutation Project	ZFIN: *sa1503*	
Genetic reagent (*Danio rerio*)	*irf8^{std96}*	(Shiau et al. 2015)	ZFIN: *std96*	
Genetic reagent (*Danio rerio*)	*rag2^{E450fs}*	(Tang et al. 2014)	ZFIN: *E450fs*	
Genetic reagent (*Danio rerio*)	*batf3^{ulb31}*	This manuscript	ZFIN: *ulb31*	
Antibody	Anti-GFP (chicken polyclonal)	Abcam	RRID:AB_300798	1:500
Antibody	Anti-Lcp1 (rabbit)	In house		1:1000
Antibody	Anti-mCherry (mouse monoclonal)	Takara Bio	RRID:AB_2307319	1:500
Antibody	Alexa Fluor 488-conjugated anti-chicken IgG	Abcam	RRID:AB_2636803	1:500
Antibody	Alexa Fluor 594-conjugated anti-rabbit IgG	Abcam	RRID:AB_2782993	1:500

Antibody	Alexa Fluor 647-conjugated anti-mouse IgG	Abcam	RRID:AB_2890037	1:500
Commercial assay or kit	SP6 RNA Polymerase	New England BioLabs	Cat# M0207	
Commercial assay or kit	High Pure PCR Cleanup Microkit	Roche	Cat# 498395500	
Commercial assay or kit	Rneasy Plus mini kit	Qiagen	Cat# 74134	
Chemical compound, drug	SYTOX™Red	Invitrogen	Cat# S34859	
Chemical compound, drug	qScript cDNA SuperMix	Quanta Biosciences	Cat# 95048-100	
Software, algorithm	Flow-Jo LLC	TreeStar	RRID:SCR_008520	
Software, algorithm	Black Zen software	Zeiss, Germany	RRID:SCR_018163	
Software, algorithm	Blue Zen software	Zeiss, Germany	RRID:SCR_013672	
Software, algorithm	R Statistical software v. 4.0.3	R Project for Statistical Computing	RRID:SCR_001905	
Software, algorithm	GraphPad Prism 8	GraphPad software, USA	RRID:SCR_002798	

971

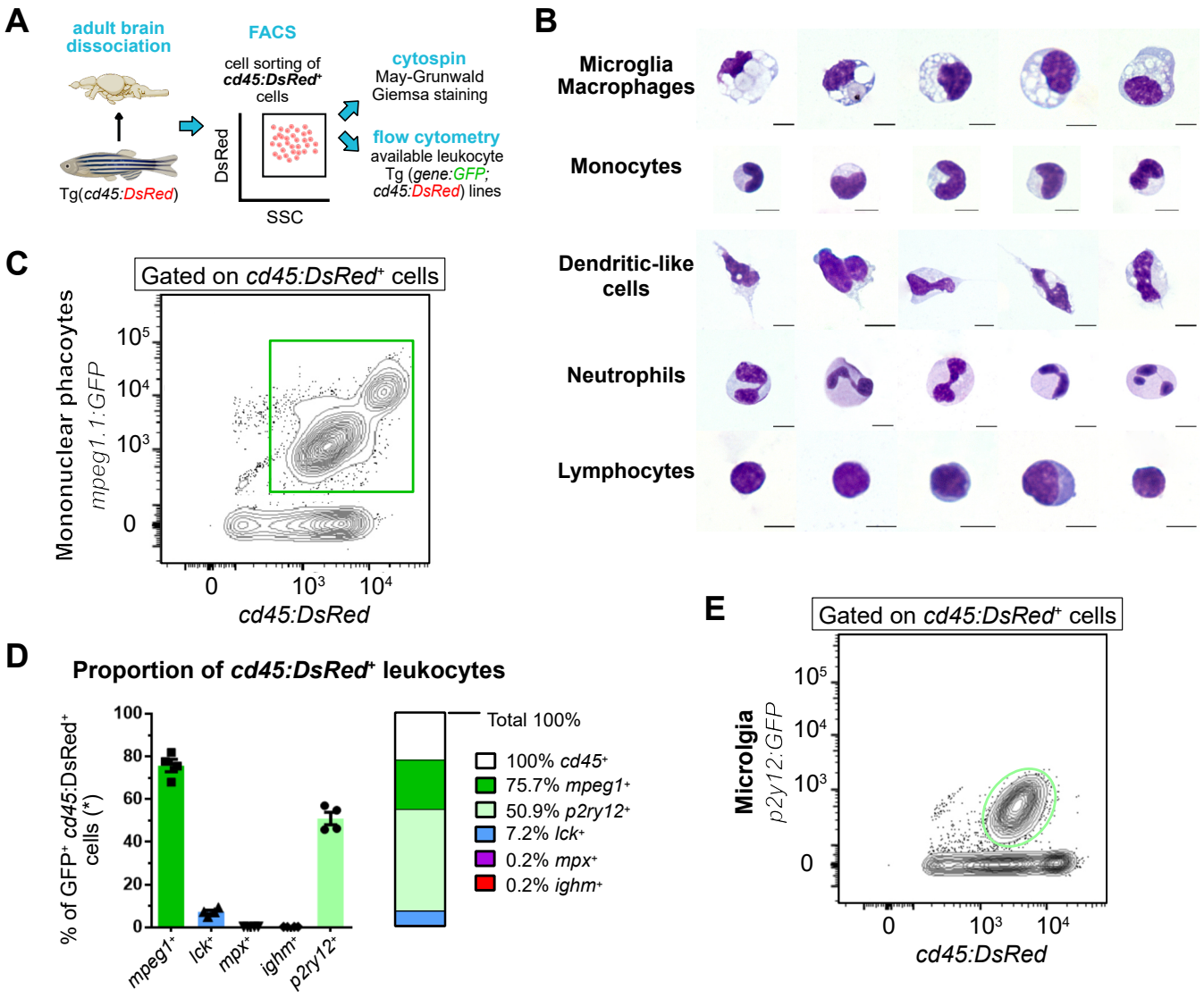

Figure 1. Leukocyte heterogeneity in the adult zebrafish brain using blood lineage-specific transgenic lines. **A.** Schematic overview of the experiment. First, *cd45:DsRed*$^+$ cells were sorted, cytospined and stained with May-Grunwald Giemsa (MGG). In parallel, lines carrying the *cd45*:DsRed transgene in combination with blood lineage-specific GFP reporters were analyzed by flow cytometry. **B.** Morphology of brain-sorted *cd45:DsRed*$^+$ cells stained with MGG. Microglia and/or macrophages, monocytes, dendritic cells, neutrophils and lymphocytes were identified. The scale bar represents 5 µm. **C.** Flow cytometry analysis on brain cell suspensions from adult *Tg(mpeg1:GFP; cd45:DsRed)* identifying *mpeg1:GFP*$^+$*; cd45:DsRed*$^+$ mononuclear phagocytes (green gate). **D.** Proportion of brain immune cell types, as determined by flow cytometry analysis on cell suspensions from fish carrying *cd45:DsRed*$^+$ and a lineage-specific GFP reporter (*n*=4 fish). The percentage relative to total *cd45:DsRed*$^+$ leukocytes is shown, with the exception of *Tg(ighm:GFP; cd45:DsRed)* which are not normalized as the *cd45:DsRed* transgene is not expressed in the B cell lineage. **E.** Flow cytometry analysis of brain cell suspensions from an adult *Tg(p2ry12:p2ry12-GFP; cd45:DsRed)* fish, identifying *p2ry12:p2ry12-GFP*$^+$*; cd45:DsRed*$^+$ microglial cells (light green gate). *n* refers to the number of biological replicates. Data in (D) are mean ± SEM.

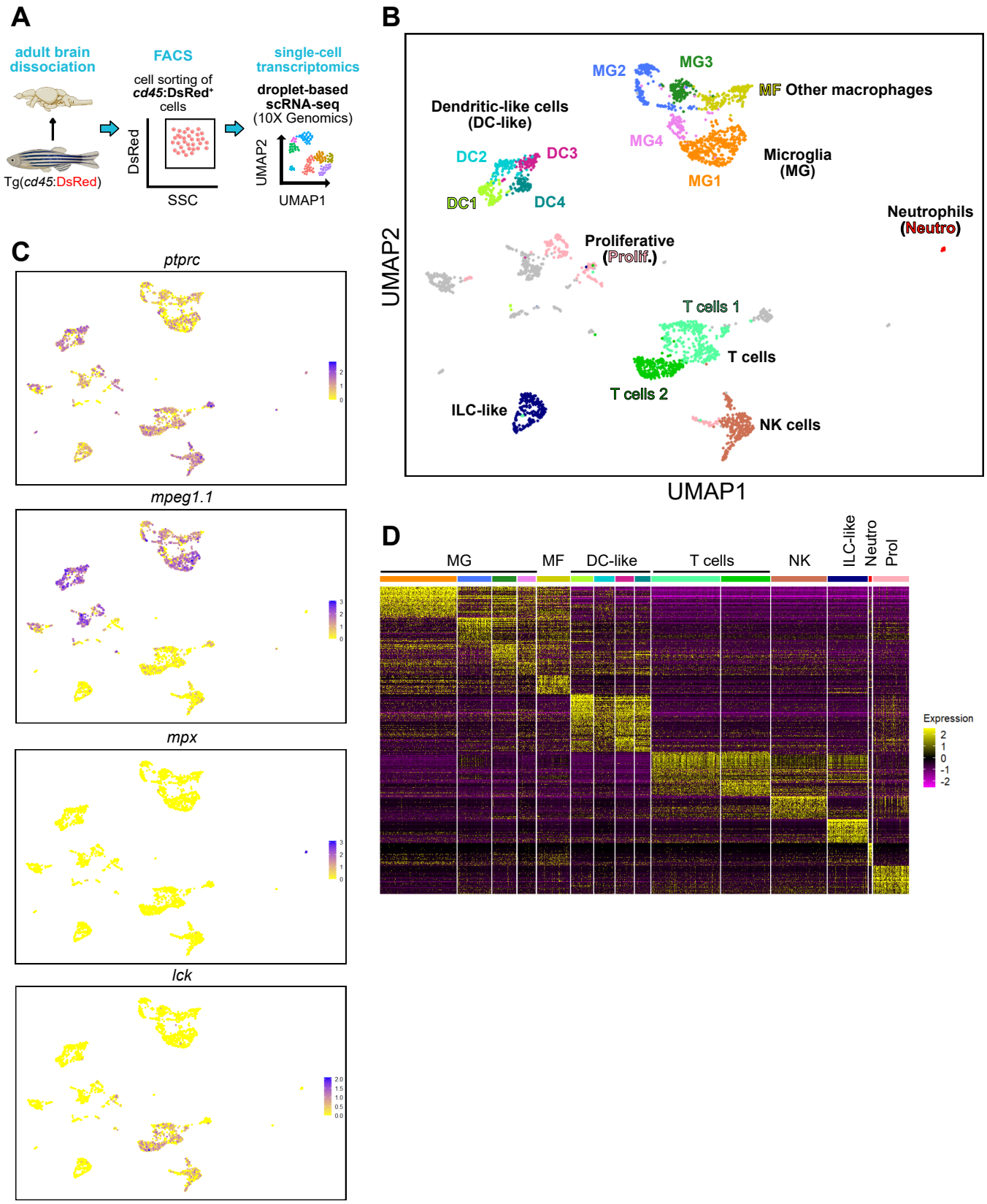

Figure 2. Diversity of brain leukocytes as shown by single-cell transcriptomics. A. Schematic overview of the experimental approach. Single-cell profiling of total brain *cd45:DsRed*$^{+}$ leukocytes (pool from 3 individual fish) was performed using the 10X Genomics platform. **B.** Split Uniform Manifold Approximation Projection (UMAP) of brain *cd45:DsRed*$^{+}$ cells with annotated cell populations. Clusters in grey shade are not indicative of a specific cell type and were not annotated. **C.** UMAP plots depicting the expression pattern of *ptprc*, also known as *cd45* (leukocytes), *mpeg1.1* (mononuclear phagocytes), *mpx* (neutrophils) and *lck* (T and NK lymphocytes). Gene expression levels from low to high are indicated by a color gradient from yellow to purple (normalized counts in log1p). **D.** Heat map of the top differentially up-regulated genes in each cluster (row=gene, column=cell type). Color scale (gradual from purple to yellow) indicates the expression level (average $\log_2$ fold change).

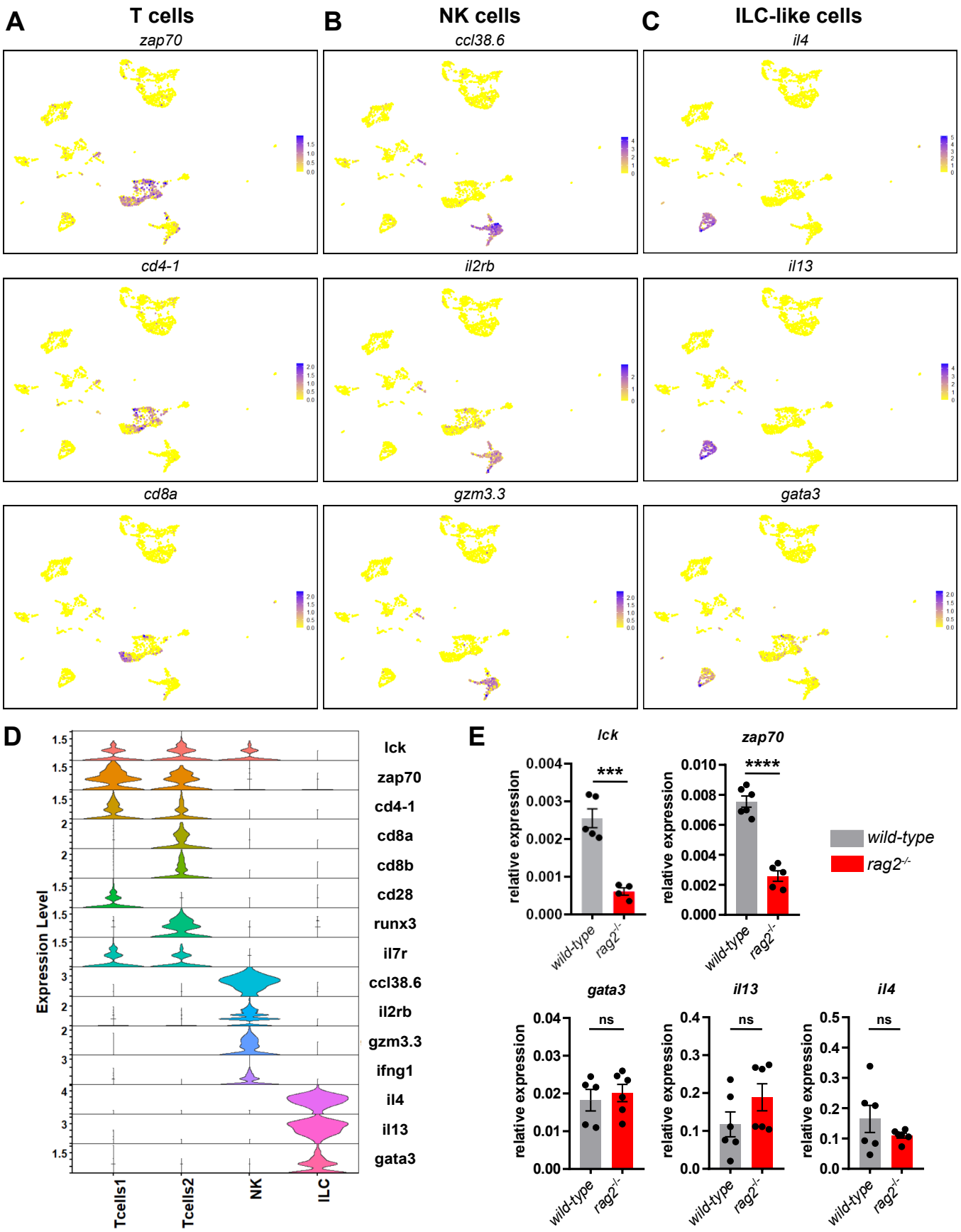

Figure 3. Single-cell RNA sequencing identifies several lymphocyte subpopulations in the adult brain. A-C. UMAP visualization of the expression of selected genes in the annotated T cell clusters Tcells1 and Tcells2 (*zap70*, *cd4-1* and *cd8a*), NK cluster (*ccl38.6*, *il2rb*, *gzm3.3*) and ILC-like cluster (*il4*, *il13* and *gata3*). Color scale (gradual from yellow to purple) indicates the expression level for each gene (normalized counts in log1p). **D.** Violin plots representing the expression levels of known lymphocyte markers (normalized counts in log1p) within the different clusters. **E.** Comparison of the relative expression of *lck*, *zap70*, *gata3*, *il13* and *il4* transcripts between brain *cd45:DsRed*$^{+}$ cells isolated by FACS from T cell-deficient *rag2*$^{-/-}$ mutants (red bars) and their *wild-type* siblings (grey bars). Each data point represents an individual fish (n=6) and error bars indicate SEM. *** P<0.001, **** P<0.0001 (Two-tailed unpaired t-test).

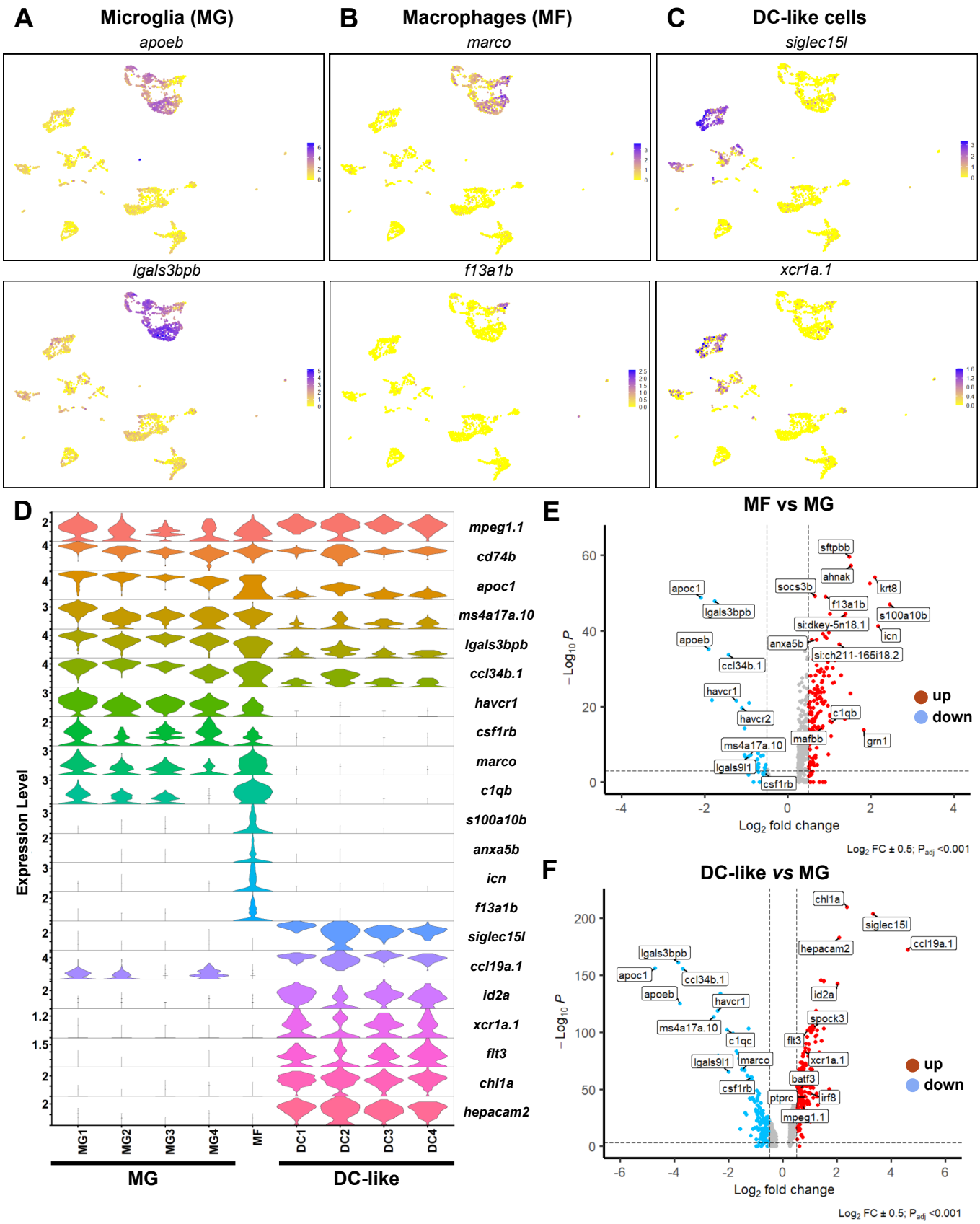

Figure 4. Heterogenous subsets of mononuclear phagocytes exist in the zebrafish brain. A-C. UMAP visualization of the expression of selected genes in the microglia (*apoeb* and *lgals3bpb*) (A), non-microglia macrophage (*marco* and *f13a1b*) (B) and DC-like (*xcr1a.1* and *siglec15l*) (C) cell clusters. Color scale (gradual from yellow to purple) indicates the expression level for each gene (normalized counts in log1p). **D.** Violin plot analysis comparing the expression levels of selected genes (y-axis, normalized counts in log1p) between the different mononuclear phagocyte cell clusters. **E.** Volcano plot showing the differentially expressed (DE) genes between microglia (MG) and non-microglia macrophages (MF). Lines indicate significantly DE genes ($\log_2$ fold-change >|0.5|, $-\log_{10}$ P_{adj} <0.001). Red dots represent up-regulated genes and blue dots down-regulated genes. Labels show representative DE genes identified in the analysis. **F.** Volcano plot showing the DE genes between microglia (MG) and DC-like cells (DC-like). Lines indicate significantly DE genes ($\log_2$ fold-change >|0.5|, $-\log_{10}$ P_{adj} <0.001).

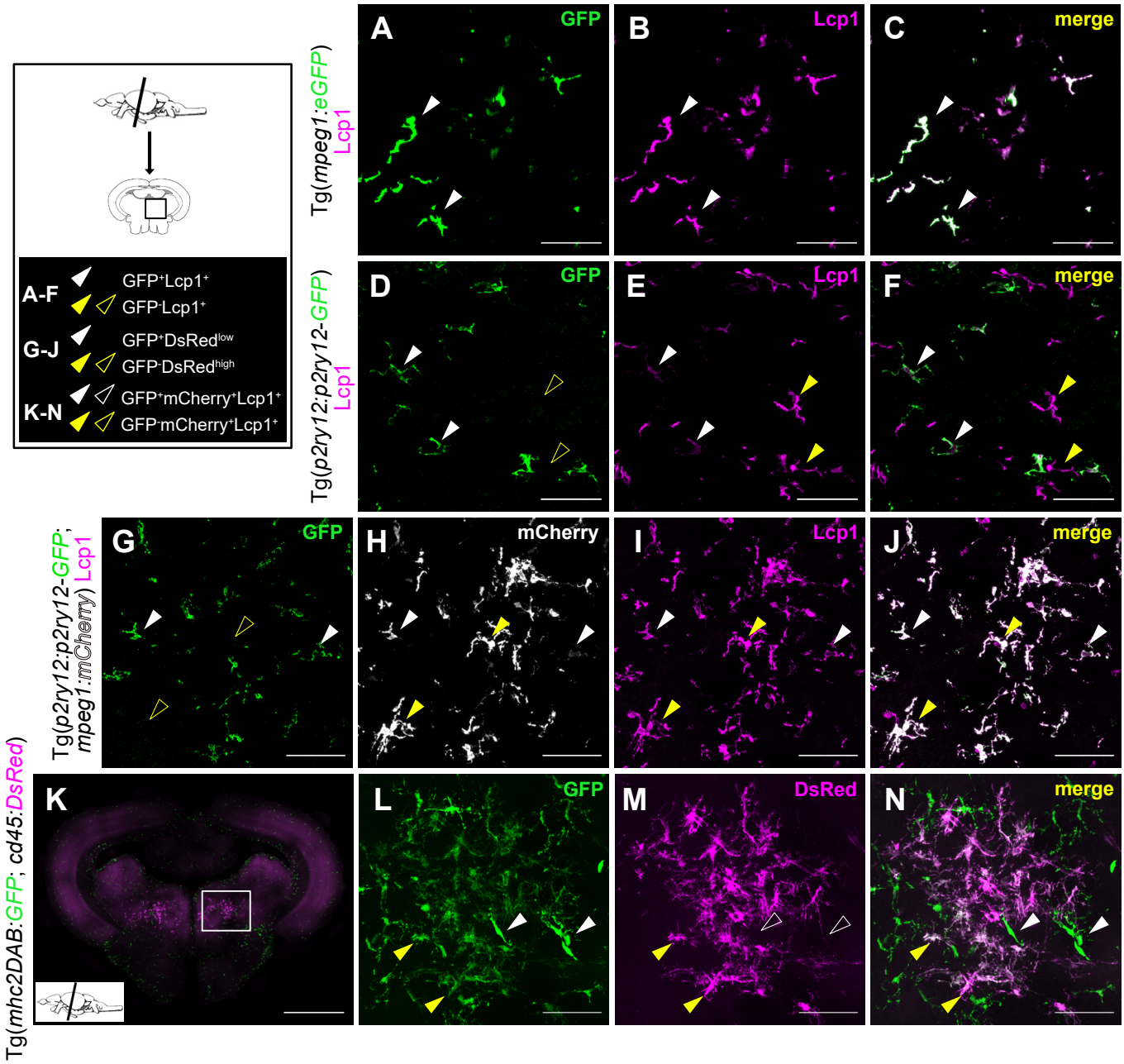

Figure 5. DC-like cells localize together with microglia within the brain parenchyma. A-F. Immunofluorescence on transversal brain sections (14 µm) from *Tg(mpeg1:GFP)* (A-C) or *Tg(p2ry12:p2ry12-GFP*) (D-F) transgenic adult fish co-immunostained with anti-GFP (green) and anti-Lcp1 (magenta) antibodies. **A-C.** All *mpeg1*:GFP$^+$ mononuclear phagocytes in the brain parenchyma display Lcp1 immunostaining, as expected. **D-F.** Similarly, all microglial cells, identified by GFP expression in the brain parenchyma of *Tg(pr2y12:p2ry12-GFP)* fish, are Lcp1$^+$, as expected. **G-J.** In sections of adult *Tg(p2ry12:p2ry12-GFP; mpeg1:mCherry)* double transgenic animals, GFP labeling is not observed in all mCherry$^+$ cells. GFP (green), mCherry (grey), Lcp1 (magenta) and merge of the three channels. All images were taken using a 20X objective and correspond to orthogonal projections. White arrowheads point to microglial cells (GFP$^+$; Lcp1$^+$or GFP$^+$; mCherry$^+$; Lcp1$^+$) and yellow arrowheads to DC-like cells (GFP$^-$; Lcp1$^+$ or GFP$^-$; mCherry$^+$; Lcp1$^+$). Scale bars: 50 µm. **L-O.** Confocal imaging of a midbrain vibratome section (100 µm) from an adult *Tg(mhc2dab:GFP; cd45:DsRed)* brain. GFP (green), DsRed (magenta) and merge of the two channels are shown. Images correspond to orthogonal projections, white arrowheads point to GFP$^+$; DsRed$^+$ cells and yellow arrowheads to GFP$^-$; DsRed^{high}. Scale bar in (K): 100 µm, scale bar in (L-N): 50 µm.

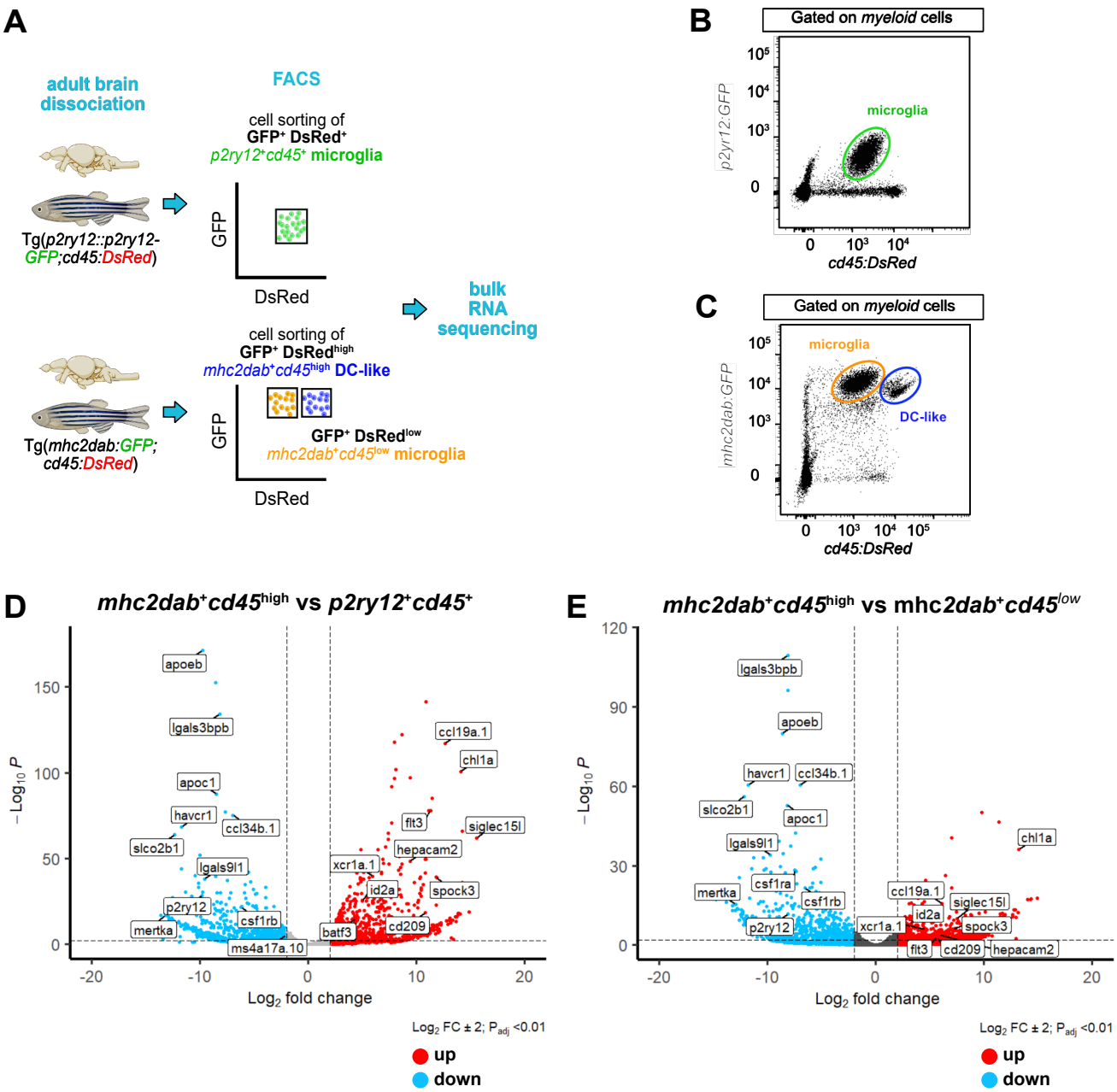

Figure 6. Transcriptomic analysis of microglia (*p2ry12⁺; cd45⁺* or *mhc2dab⁺; cd45^{low}*) and DC-like cells (*mhc2dab⁺; cd45^{high}*). A. Schematic overview of the experiments. Microglia were isolated using *Tg(p2ry12:p2ry12-GFP; cd45:DsRed)* or *Tg(mhc2dab:GFP; cd45:DsRed)* transgenic fish, and DC-like cells using the *Tg(mhc2dab:GFP; cd45:DsRed)* reporter line. **B.** Representative flow cytometry plot identifying microglial cells in brain cell suspensions from *Tg(p2ry12:p2ry12-GFP; cd45:DsRed)* fish. **C.** Representative flow cytometry plot identifying *mhc2dab:GFP⁺; cd45:DsRed^{low}* microglia from *mhc2dab:GFP⁺; cd45:DsRed^{high}* DC-like cells in brain cell suspensions from *Tg(mhc2dab:GFP; cd45:DsRed)* fish. **D.** Volcano plot showing the differentially expressed (DE) genes between *mhc2dab⁺; cd45^{high}* DC-like cells and *p2ry12⁺; cd45⁺* microglia. Red dots represent up-regulated genes and blue dots down-regulated genes. Lines indicate significantly DE genes ($\log_2$ fold-change >|2|, $-\log_{10}$ P_{adj} <0.01). Labels show marker genes for DC-like cells and microglia identified in the scRNA-sequencing analysis. **E.** Volcano plot showing the DE genes between *mhc2dab⁺; cd45^{high}* DC-like cells (blue) and *mhc2dab⁺cd45^{low}* microglia (red). Lines indicate significantly DE genes ($\log_2$ fold-change >|2|, $-\log_{10}$ P_{adj} <0.01).

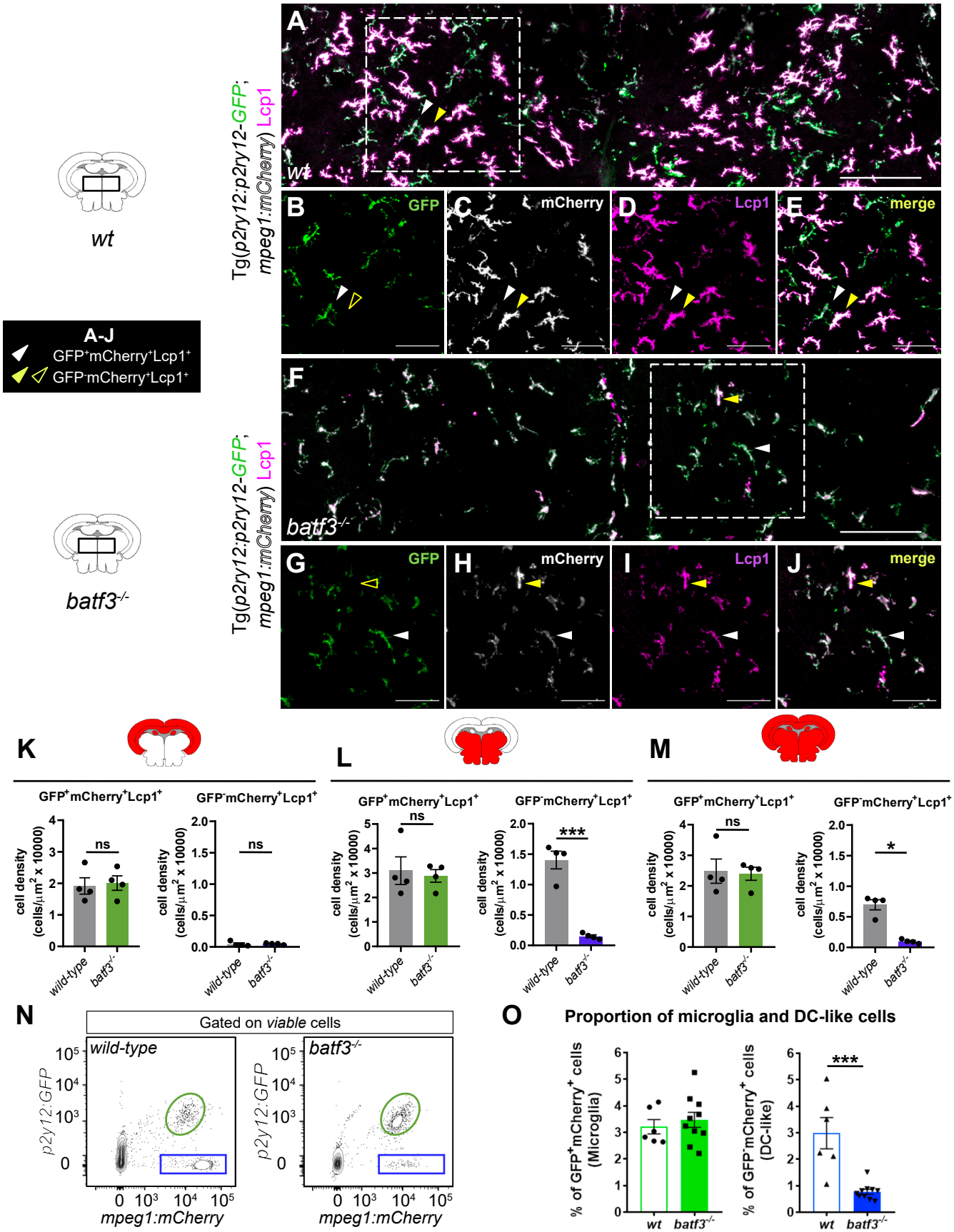

Figure 7. Brain DC-like cells are lost in *batf3*$^{-/-}$ mutant fish. A-J. Immunofluorescence on transverse brain sections (14 µm) from adult *wild-type* (A-E) and *batf3*$^{-/-}$ mutant (F-J) fish carrying the *Tg(p2ry12:p2ry12-GFP; mpeg1:mCherry)* double transgene and immunostained for GFP (green), mCherry (grey) and Lcp1 (magenta). Illustrative case of the merge of the three channels (A, F) allowing to identify GFP^{+}; mCherry^{+}; Lcp1^{+} microglia (white arrowheads) versus GFP^{-}; mCherry^{+}; Lcp1^{+} DC-like cells (yellow arrowheads). While DC-like cells are found in high numbers within the ventral part of control parenchyma (A), these are dramatically decreased following genetic loss of *batf3* (F). Scale bars: 100 µm. (B-E, G-J). Single channels high magnification of the insets in A (B-E) and F (G-J). Scale bars: 50 µm. Images were taken using a 20X objective and correspond to orthogonal projections. **K-M.** Quantification of cell density for GFP^{+}; mCherry^{+}; Lcp1^{+} microglia and GFP^{-}; mCherry^{+}; Lcp1^{+} DC-like cells in the dorsal midbrain area or optic tectum (K), ventral midbrain area (L) and the entire section (M) of control (grey bars) and *batf3*$^{-/-}$ (green bars) fish. Each dot

represents a single fish and data are mean ± SEM. * P<0.05 (Mann-Whitney test), *** P<0.0001 (Two-tailed unpaired t-test). **N.** Flow cytometry analysis of brain cell suspensions from *wild-type* and *batf3*$^{-/-}$ adult fish carrying the *Tg(p2ry12:p2ry12-GFP; mpeg1:mCherry)* reporter. The GFP^{+}; mCherry^{+} fraction identifies microglia (green circle), whereas the GFP^{-}; mCherry^{+} fraction contains mainly DC-like cells (blue frame). **O.** Percentage of microglia and DC-like cells in brain cell suspensions for each genotype, relative to the whole living brain population, as shown in (N) (*wild-type*, *n*=6; *batf3*$^{-/-}$, *n*=10). *** P<0.001 (Two-tailed unpaired t-test). *n* refers to number of biological replicates.

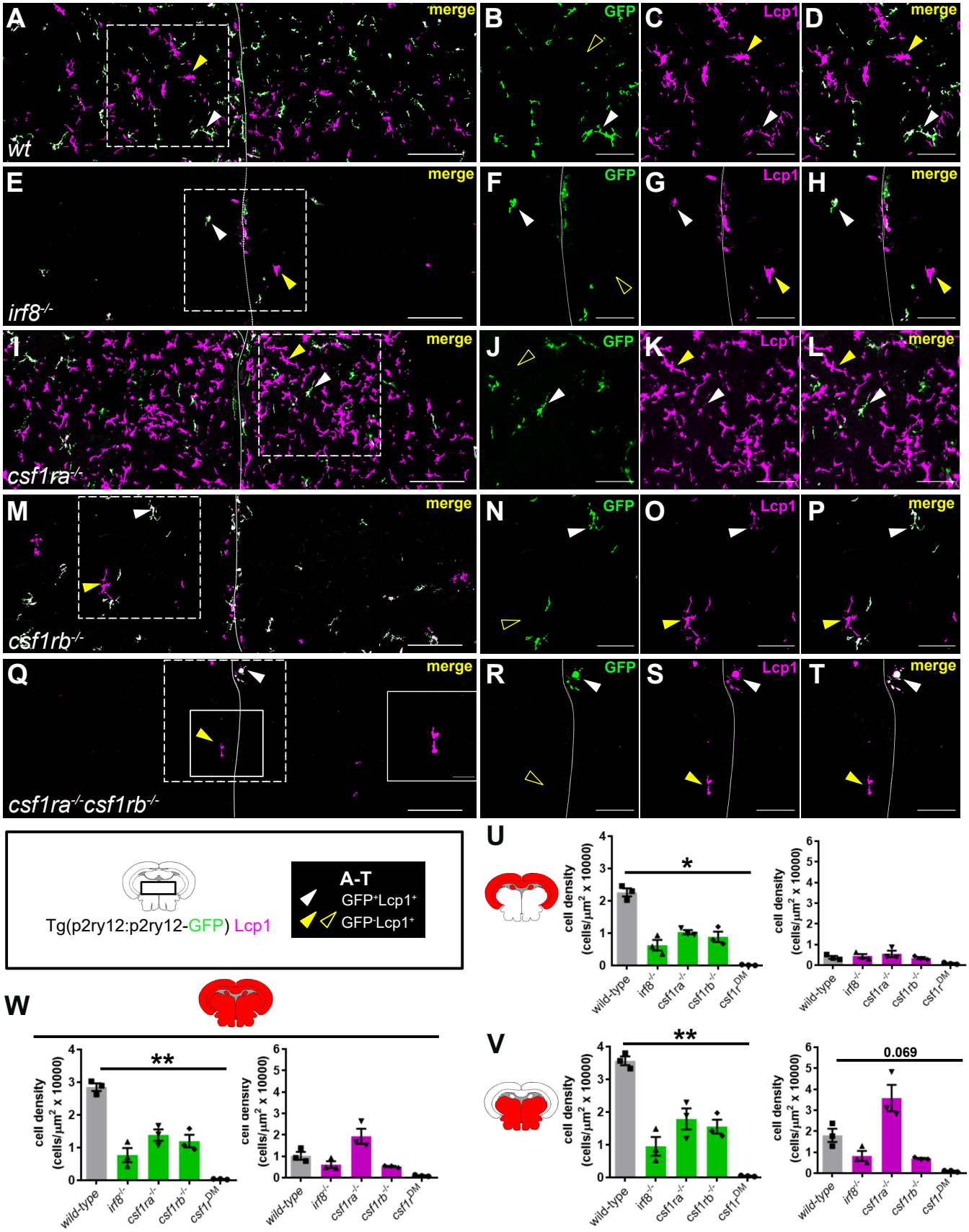

Figure 8. Examination of microglia and DC-like cells in myeloid–deficient mutant lines. A-D. Immunofluorescence on transverse brain sections from *Tg(p2ry12:p2ry12-GFP)* transgenic adult *wild-type* (A-D), *irf8*$^{-/-}$ (E-H), *csf1ra*$^{-/-}$ (I-L), *csf1rb*$^{-/-}$ (M-P) and *csf1ra*$^{-/-}$*; csf1rb*$^{-/-}$ *(csf1r*^{DM}*)* (Q-T) fish, co-stained with anti-GFP (green) and Lcp1 (magenta) antibodies. **A, E, I, M, Q.** For each genotype, illustrative case of the merge of the two channels , allowing to discriminate in the parenchyma GFP^{+}; Lcp1^{+} microglia (white arrowheads) from GFP^{-}; Lcp1^{+} DC-like cells (yellow arrowheads). Single channels high magnification of the insets (dashed frame) in A (B-D), E (F-H), I (J-L), M (N-P) and Q (R-T). Outline yellow arrowheads indicate the absence of GFP signal in corresponding yellow arrowhead pointed cells. Scale bar in (A), (E), (I), (M) and (Q) represents 100 µm and scale bar in other images 50 µm. **U-V.** Quantification of the cell density for GFP^{+}Lcp1^{+} microglia and GFP^{-}Lcp1^{+} DC-like cells in the dorsal (U), ventral (V) and whole area (W) of the brain for each genotype (*n*=3). Data in U-W are mean ± SEM. *P<0.05 , **P<0.01 (Klustal-Wallis test with Dunn's post-hoc).